Summer 8-20-2023

OBSERVATIONS OF 25 GHz METHANOL MASERS IN W51A

Peter Wagstaff
DePaul University, PWAGSTAF@depaul.edu

OBSERVATIONS OF 25 GHz METHANOL MASERS IN W51A

A Thesis

Presented in

Partial Fulfillment of the

Requirements for the Degree of

MASTER OF SCIENCE

July, 2 0 2 3

BY

Peter Wagstaff

DEPARTMENT OF PHYSICS & ASTROPHYSICS

College of Science and Health

DePaul University

Chicago, Illinois

ACKNOWLEDGEMENTS

First and foremost, I thank my advisor Dr. Anuj Sarma for sharing his wealth of knowledge and resources, including the observational data for this research. Without Dr. Sarma's mentorship, patience, and support this work would not be possible. The late hours and weekends that Dr. Sarma has contributed to me alone speaks to the level of effort and dedication shown to every individual student of his. Next, I thank Dr. Bernhard Beck-Winchatz for his time as a committee member and for being the first to welcome me into the department in his role as the graduate program director. I also thank Dr. Eric Landahl for his time as a committee member as well as a mentor in the classroom. I thank Dr. Emmanuel Momjian of the National Radio Astronomy Observatory as a research collaborator and for his work editing and calibrating the observational data. I thank all my professors who have taught me and who I have assisted. I thank Dr. Susan Fisher for her hard work organizing and coordinating the teaching assistants each year. I especially thank the department chair, Dr. Jesús Pando, and other supporters working toward a more diverse and inclusive academic future. Of course, I thank the remainder of faculty and staff in the Department of Physics and Astrophysics. I thank my classmates, graduates and those who are still working toward their own goals, for their constant inclusion, encouragement, and friendship. I thank my students for new challenges and perspectives. Lastly, I thank my family past and present for their love every single day. I thank my mother, father, sisters, and brothers. I thank Mikaelah Taylor and their family as my own.

TABLE OF CONTENTS

LIST OF FIGURES

LIST OF TABLES

ABSTRACT

High mass stars are important because they alone are responsible for creating the heavy elements in the Universe. The observation of high mass star formation remains a challenging problem in astronomy because high mass stars form in densely clustered environments at large distances from us. Therefore, high angular resolution observations are required to unravel the action taking place in these dense environments. Masers can be used to observe distant regions with high angular resolution because masers are compact and bright sources. Class I methanol masers are believed to form in outflows from protostars where the shock generated by the outflowing material impacts ambient interstellar material. W51A is one of the brightest infrared sources in our Galaxy and is known to host several sites of high mass star formation. This thesis presents spectral line observations at 25 GHz toward W51A. Only one Class I methanol maser was observed at 24.959 GHz; it has a counterpart at 25.018 GHz with which it is coincident in position and velocity. Significantly, even though there is 44 GHz methanol emission very close to this position which could be a maser or thermal emission or a combination of both, it is at a different center velocity and does not share the same velocity extent as the 25 GHz masers. We interpret this to mean that the 44 GHz emission is from a different parcel of gas. There is also 36 GHz methanol emission with the same velocity extent as the 44 GHz emission. The 36 GHz emission is likely thermal but could also have weak maser emission superimposed on it. Comparison to archival data for 88 known Class I CH_3OH masers at 24.959 and 25.018 GHz reveals that the 25 GHz masers observed for this thesis are comparatively lower in intensity; 38 out

of the 88 in the archival data have intensities lower than 0.5 Jy beam^{-1}. The 25 GHz masers in W51A are located in a relatively uncrowded region with no known infrared counterparts. There is no H_2O or 1720 MHz OH maser coincident with the 25 GHz CH_3OH maser position; both of these are known to be collisionally excited like the 25 GHz masers. The nearest water maser is 0.14 pc to the north, and the closest 1720 MHz OH maser is 0.3 pc to the north and east. The nearest 6.67 GHz Class II CH_3OH maser is located 0.24 pc to the north and east of the 25 GHz CH_3OH maser position. This leads us to propose two scenarios. In the first, the 25 GHz CH_3OH masers are pumped in an outflow arising from a protostar located near the 6.67 GHz Class II CH_3OH maser position; there are two radio continuum sources e1 and e3 in the immediate vicinity of the 6.67 GHz Class II maser that could be the location of the protostar. This would imply that 25 GHz CH_3OH masers occur later in the star formation process, after the high mass protostar has formed an ionized hydrogen region. In the second scenario, the 25 GHz CH_3OH masers form very early in the star formation process and are being excited in the outflow from a hitherto unrevealed high mass protostar.

CHAPTER 1

Introduction

The formation process of high mass stars ($M > 8M_{\odot}$) is an active field of study in astronomy and astrophysics (MacKay et al. 2023). High mass stars are an important population of objects in the universe because of their role in the creation and distribution of heavy metals throughout space (Eldridge & Stanway 2022). While high mass stars may be some of the most luminous objects in the sky, the regions where they form are not always easily observed (Zinnecker & Yorke 2007). Most high mass stars form in dense clusters far away from us. The key to observing such a busy region is to achieve a high angular resolution. Radio interferometers such as the Karl G. Jansky Very Large Array (VLA) allow us to observe these regions at high angular resolution. Masers are bright, compact sources that can be resolved at great distances to probe the environment in which they are occurring (Richards et al. 2020). Class I methanol (CH_3OH) masers are commonly found offset from protostars and are thought to exist on the front of a shock caused by outflows from the star formation process (Leurini et al. 2016). The more we know about such masers, the more valuable they become as tracers of the various stages of the high mass star formation process. This thesis presents observations of 25 GHz Class I CH_3OH masers toward the high mass star forming region W51A with the aim of learning more about such masers and the regions in which they form.

The giant molecular cloud W51A contains some of the most active high mass star forming regions in our Galaxy (Ginsburg et al. 2016). It is an attractive laboratory for investigating the star formation process because it is located in a relatively isolated region of our Galaxy where there is little background or foreground emission. However, its large distance from us requires a high angular resolution for detailed observation. Hot cores exhibiting a rich spectrum of molecular emission, strong H_2O and CH_3OH masers, bright infrared sources, and numerous ultracompact and hypercompact ionized hydrogen regions are a testament to the prevalence of significant ongoing star formation activity in this region.

This thesis reports on observations of Class I CH_3OH masers at 24.959 GHz and 25.018 GHz toward W51A. Masers, their formation, molecules that emit astronomical maser radiation, and methanol masers are discussed in Section 1.1. The W51 region, and specifically W51A, are discussed in Section 1.2. This thesis uses data observed with the VLA and archival data compiled from the literature; the VLA observations and data analysis and the archival data are described in Chapter 2. The results are presented in Chapter 3 and discussed in Chapter 4. Chapter 5 presents the conclusions and discusses future work.

1.1 Masers

The Microwave Amplification of the Stimulated Emission of Radiation (MASER) is a physical phenomenon which occurs given the correct conditions which are presented in detail in Section 1.1.1, resulting in a directional beam in the microwave regime of electromagnetic radiation. The word maser is used in its own right like the common terminology of the laser. Masers and lasers are analogous in their physical production mechanism, with the main distinction being the range of the wavelengths of the

emitted radiation. Both can be created in a laboratory. However, the existence of masers in nature and the detection of astronomical masers provides a rich field of research for astronomy and astrophysics. Understanding maser formation from observational and theoretical perspectives can provide insight to the regions of the universe in which masers are observed and detected. The formation of masers and molecules that are known to form masers in astrophysical environments is discussed in more detail in the following subsections, followed by a discussion of methanol masers and their classification into Class I and II types.

1.1.1 Maser Formation

The criteria to be met for maser formation include population inversion, stimulated emission, and amplification. The initial need of population inversion introduces the concept of pumping. A typical population of molecules is usually expected to have a larger number of molecules in a lower energy state, and in contrast an inverted population has a larger number of molecules in a higher energy state. Such a population-inverted state is shown in the left panel of Figure 1.1.

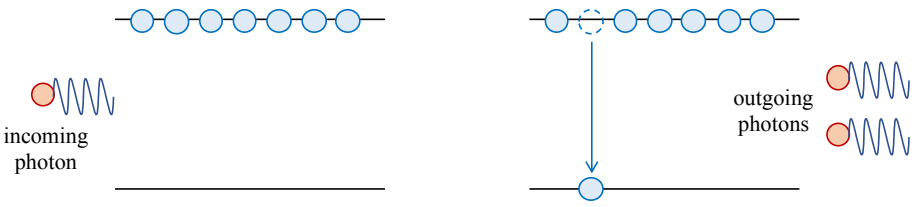

Figure 1.1: Figure showing population inversion and stimulated emission.

Naturally or without outside influence, it is expected that a population tends toward the state of lowest energy. To achieve a majority of molecules in a higher energy

state a mechanism continually imparting energy must exist, and this mechanism is referred to as pumping. The two possibilities of astronomical pumping mechanisms to satisfy the population inversion condition are collisional and radiative. When molecules collide and impart energy, they can be excited to a higher energy state and are said to undergo collisional pumping. Examples of collisional pumping are seen in the outflows of matter from star forming regions interacting with the surrounding ambient interstellar medium. The second case of pumping is from radiation or photons imparting energy on the population to excite the molecules to a higher energy state. Examples of radiative pumping are seen around radiative host protostars. A pumping mechanism may occur periodically on some timescales, or it must occur at a higher rate than any de-excitation occurring in order to reach a population inversion. Similarly, if a single event pumps the molecules, then it must be at a scale great enough to reach a population inversion. With a sufficient pumping mechanism the majority of molecules can exist in the excited state satisfying population inversion, and the next step of maser formation has the chance to occur. Stimulated emission occurs when a specific frequency of incident photon interacts with the excited molecule to lower its energy level and emit a photon of the exact same frequency, as shown in Figure 1.1. The two identical, coherent photons then have the chance to continue the process of stimulated emission on other molecules resulting in four photons of the same frequency. Continuing this trend there will be eight identical photons, and then there are sixteen identical photons. Thus, amplification by powers of two has occurred, and the final need for the formation of a maser has been met. Lasers or masers in the laboratory take advantage of mirrors to build up this amplification process. In star forming regions, masers require a column of velocity-coherent gas. Velocity coherence means that the phase of the photons traveling in the gas are preserved. This is important because as noted above, the stimulated emission needs the outcome of two identical, coherent photons

to be emitted for amplification to continue along the path of the maser. Velocity coherence may only exist along a certain long, narrow path of gas which allows the maser amplification. This explains why masers are observed as bright, point-like sources in the sky.

1.1.2 Astronomical Masers

Astronomical masers can occur from the transitions of several molecules, including OH, H_2O, CH_3OH, SiO, NH_3 and H_2CO (e.g., Elitzur 1992). Maser emission from these molecules can be emitted over a wide range of frequencies from $\sim$1 GHz to hundreds of GHz, even for the same molecule. For example, although the most commonly observed H_2O maser line is at 22 GHz, mm and submm H_2O masers have been observed at 183, 321, 325, and 658 GHz (e.g., Baudry et al. 2018, and references therein). Astronomical masers form in a wide variety of environments ranging from star forming regions, to evolved stars (e.g., in the red giant phase), and even toward the centers of galaxies (Reid & Moran 1981; Hagiwara et al. 2016). They are a very useful tool because they are compact and bright sources. The availability of receivers on interferometers capable of observing masers at a vast array of frequencies allows them to be used as probes of a variety of environments at high angular resolution (Richards et al. 2020).

1.1.3 Methanol Masers

The methanol (CH_3OH) molecule is responsible for maser transitions at several different frequencies. Once a reasonably sized sample of these masers had been observed, it became clear that CH_3OH maser emission consists of two classes (Batrla et al. 1987; Menten 1991). Masers that had been found offset from centers of star

formation activity such as ultracompact H II regions were classified as Class I CH_3OH masers, whereas masers that appeared to coincide with ultracompact H II regions and other star formation indicators were classified as Class II CH_3OH masers. Today we know that these two classes of masers differ in more than just the locations in which they are found. Class I masers are collisionally excited whereas Class II masers are radiatively excited (Cragg et al. 2005; Leurini et al. 2016). In fact it is because of these different excitation pathways that the two classes of masers are found in different locales. Collisional excitation of Class I CH_3OH masers takes place in the outflows in star forming regions, in shocked material where the outflow from the protostar rams into ambient interstellar material. In contrast, excitation of Class II masers is caused by radiation from the protostar and hence these masers form closer to the protostar.

A significantly larger effort has gone into observing Class II CH_3OH masers compared to Class I masers (e.g., Nguyen et al. 2022, and references therein). This was likely due to the fact there are many strong Class II CH_3OH masers at 6.7 GHz, a lower frequency for which receivers were available on several radio telescopes, and observable even in less than optimum atmospheric conditions. Moreover, the fact that they occur so close to the protostar makes them an effective tracer of the conditions in these regions at resolutions not achievable for any thermal lines. Observations of several Class II CH_3OH maser sources were also carried out at 12.2 GHz (Goedhart et al. 2005), although in modern times, this is no longer the case due to radio frequency interference from satellite downlink signals that sit very close to the 12.2 GHz frequency window. With the introduction of 44 GHz receivers on the VLA, the field of Class I maser observations made substantial progress (Kogan & Slysh 1998), which was accelerated even more when 36 GHz receivers become available on the VLA (Sjouwerman et al. 2010). A significant number of 44 GHz and 36 GHz CH_3OH maser observations have also been carried out with ATCA, the Australia Telescope

Compact Array (Voronkov et al. 2014). Although the most commonly observed Class I CH_3OH maser transitions today are 44 GHz and 36 GHz, the discovery of Class I maser emission from methanol was in the 25 GHz series of lines toward the Orion-KL region (Barrett et al. 1971). The 25 GHz masers may be rarer than the 44 GHz and 36 GHz masers. Since so little is known about these masers, this thesis presented an unique opportunity to look for them in the environment of a high mass star forming region.

1.2 The W51 Region

W51 is a giant molecular cloud and star forming region, ranking among the most massive ($M > 10^6 M_\odot$) and active high mass star forming regions in our Galaxy (Eden et al. 2018). Its location in an isolated region of the Galaxy near $l = 49.5°$ and $b = -0.4°$, where there is little background or foreground emission, makes it an attractive laboratory to investigate high mass star formation (Ginsburg et al. 2017), but its relatively large distance at 5.4 kpc (Sato et al. 2010) demands high angular resolution observations. Early observations of W51 at 430 MHz showed that it is comprised of four large ($\sim 10'$ - $20'$) radio components which were named A through D (Kundu & Velusamy 1967); three of these regions are shown in Figure 1.2. Of these, W51A is the focus of this thesis, and is discussed in more detail in Section 1.2.1 below.

1.2.1 W51A

W51A is among the three most luminous regions of our Galaxy at infrared wavelengths emitted by dust, the other two being W49A and Sgr B2. It contains two

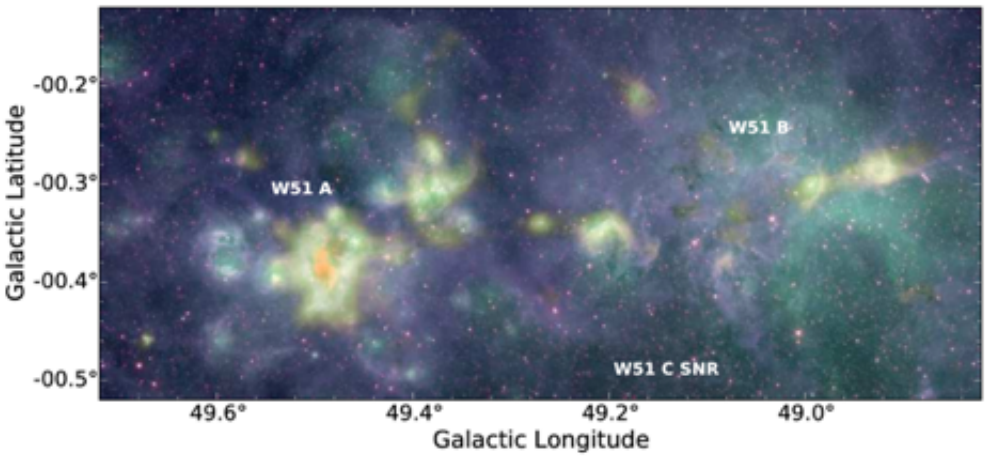

Figure 1.2: Figure taken from Ginsburg et al. (2015) showing three of the four radio components A-D in W51. The blue, green, and red colors in the image are observations in bands 1, 3, and 4 (corresponding to wavelengths of 3.4, 12, and 22 μm respectively) made with the Wide-field Infrared Survey Explorer (WISE) space telescope. The yellow-orange semitransparent layer is from the 1.1 mm Galactic Plane Survey data taken with the Bolocam camera on the Caltech Submillimeter Observatory. Finally, the faint whitish haze filling in most of the image is from a 90 cm VLA image, which primarily traces the W51 C supernova remnant.

regions that are among the few that have the potential to form high mass clusters in our Galaxy (with $M > 10^4 M_\odot$). Tracers of star formation activity are abundant in W51A, including hot cores exhibiting rich molecular spectra, strong H_2O and CH_3OH masers, bright infrared (IR) sources, and ultracompact (UC) and hypercompact (HC) ionized hydrogen (H II) regions. In their mid-infrared (MIR) observations, Lim & De Buizer (2019) found 41 objects that are likely to be massive young stellar objects (MYSOs). About 20 of these do not correspond to detectable radio continuum sources at centimeter wavelengths, indicating that they are at a very early stage in their formation process.

W51A was further resolved into two components labeled G49.5−0.4 and G49.4−0.3 by Wilson et al. (1970). An image delineating the regions covered by these two components is shown in Figure 1.3. Radio continuum emission from G49.5−0.4 at cm wavelengths revealed that it is comprised of several regions labeled a, b, c, and so on (Mehringer 1994). Note that the same letter designations (a, b, . . .) are also used for regions in G49.4−0.3, but henceforth in this thesis, all references to a, b, and so on, will be to the regions in G49.5−0.4. Two of these regions, e and d, represent the two brightest radio continuum emission sources in G49.5−0.4.

At infrared wavelengths, Wynn-Williams et al. (1974) found two bright components in G49.5−0.4; they are IRS 1, which is coincident with radio source e, and IRS 2, which is coincident with radio source d. The locations corresponding to these two infrared sources are shown in Figure 1.4. Also marked in this figure are the sources e1, e2, and e3. The source e2, sometimes called W51e2, is the brightest compact source in the region and is comprised of at least two sources, an HC H II region e2w, and a hot molecular core e2e (Goddi et al. 2016). Sources e1 and e3 are marked in Figure 1.4 because they are nearest to the 25 GHz masers observed for this thesis; both sources will be discussed in more detail in Section 4.4.

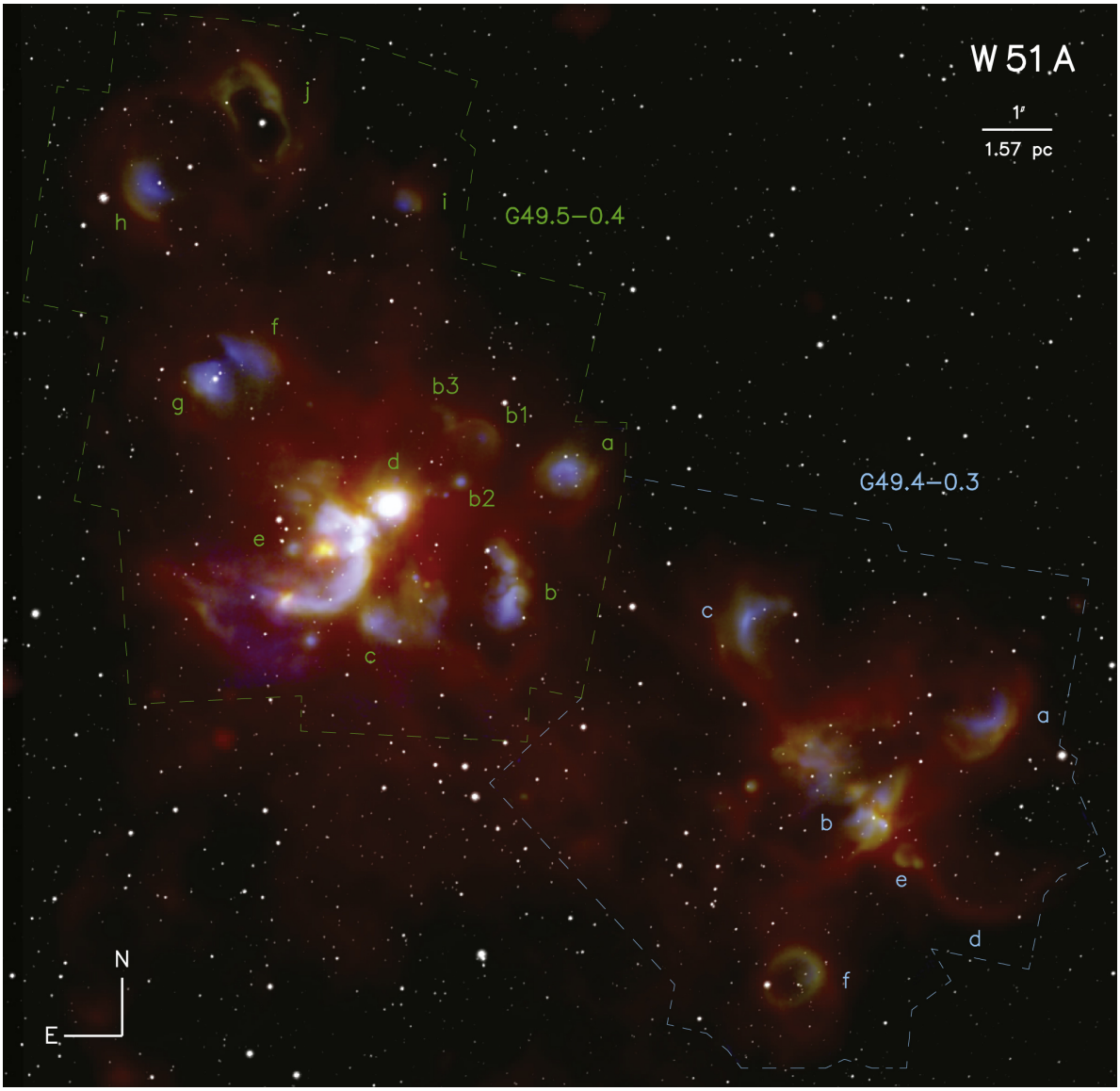

Figure 1.3: Figure taken from Lim & De Buizer (2019) showing a 3-color image of W51A. Blue is a 20 μm image and green is a 37 μm image, both taken with the Stratospheric Observatory For Infrared Astronomy (SOFIA) instrument FORCAST (Faint Object InfraRed CAmera for the SOFIA Telescope), and red is a 70 μm image taken with the Herschel Space Observatory. Overlaid in white is the Sloan Digital Sky Survey (SDSS) star field observed in the z-band (0.9134 μm), which traces both stars in the W51A region and field stars. The green dashed lines delineate the area of the subcomponent G49.5−0.4, and blue dashed lines delineate G49.4−0.3.

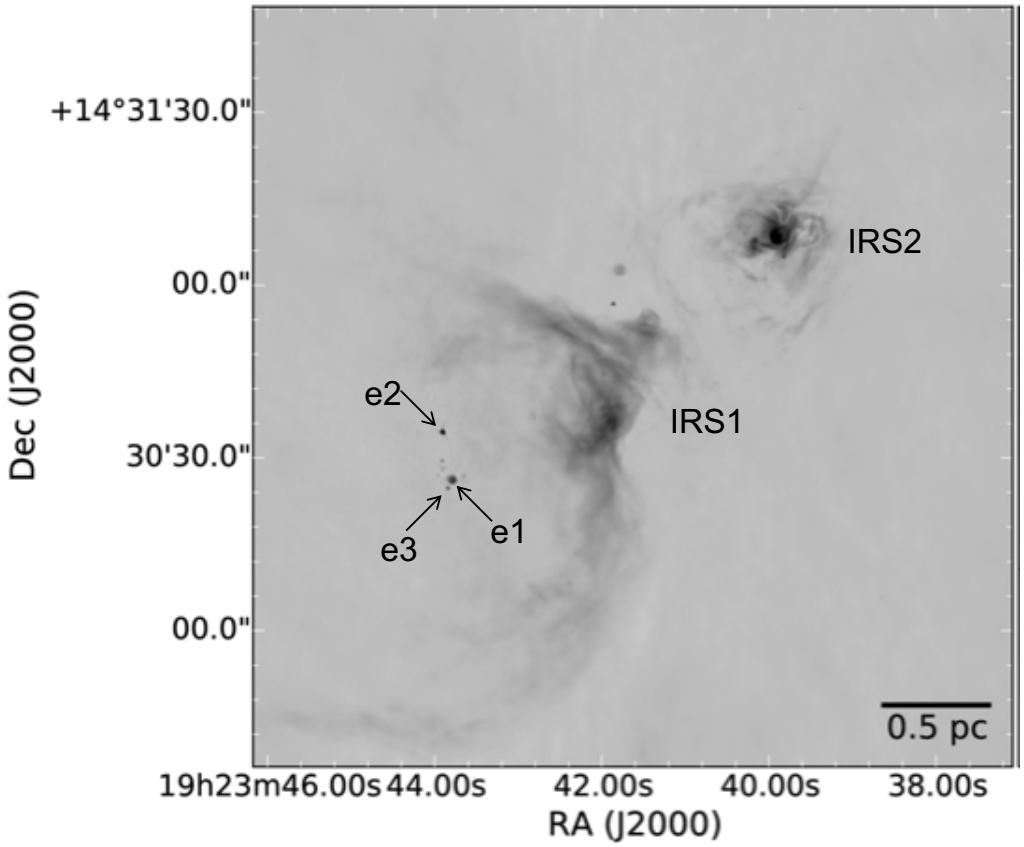

Figure 1.4: Figure taken from Ginsburg et al. (2016) showing a VLA image of W51A at 14.5 GHz. Some of the prominent sources mentioned in Section 1.2.1 are marked in this figure.

CHAPTER 2

Observations and Data Reduction

This thesis uses data observed with the Karl G. Jansky Very Large Array (VLA) and archival data compiled from the literature. The VLA observations and data analysis are described in Section 2.1. The archival data were obtained from the website `maserdb.net` and are described in Section 2.2.

2.1 VLA Observations

The Class I CH_3OH maser observations described in this thesis toward the molecular cloud complex and high mass star forming region W51A were observed with the VLA on 2016 July 31 (proposal code: VLA/16A-494; PI: A. P. Sarma). The VLA is located in the Plains of San Agustin in New Mexico, United States. Radio telescopes can come in two types: single dish and interferometers, depending on the observational needs. The key difference between the two is the angular resolution achieved to resolve the target in the sky. The angular resolution of a telescope is the smallest separation that two objects in the sky can be while still being distinguishable. Angular resolution depends on the wavelength of light being observed and the size or diameter of the telescope. It can be calculated as $\theta \approx \lambda/D$ where θ is the angular resolution in radians, λ is the wavelength of light, and D is the diameter of the single dish or the largest distance between two antennae of an interferometer. Therefore, for single dish radio telescopes the diameter of the dish must be increasingly larger

to achieve higher angular resolution, and at some point, it becomes unfeasible in terms of engineering. Instead, interferometers like the VLA consist of a number of single dishes (also referred to as antennas). The signals received by each antenna in the interferometer are combined to achieve high angular resolution. The VLA was designed so that its antennas can be moved along railway tracks and arranged farther apart to increase D, the largest separation of two antennae; these separations between antennas are also referred to as baselines. There are four configurations that these antennas can be arranged in; they are called A, B, C, and D. Each configuration uses the same antennas arranged in a Y shape, but the distances between the antennas are varied with A being the largest baseline at 36.4 km and D being the smallest baseline at 1.03 km. Since the angular resolution goes as λ/D, the A configuration of the VLA will have the highest angular resolution at a given wavelength, and the D configuration will have the lowest angular resolution.

The observations at 25 GHz reported in this thesis were carried out in the B configuration of the VLA. The observational parameters are listed in Table 2.1. The 25 GHz frequency of our observations corresponds to a wavelength of 0.012 m. The maximum separation between antennas in the B configuration of the VLA is 11.1 km. Using

$$\theta \text{ (resolution in radians)} = \frac{\lambda}{D}$$

we find that the angular resolution is 1.08×10^{-6} radians. Multiplying by $180 \times 3600/\pi$ to convert to arcseconds, the angular resolution in the B configuration of the VLA is found to be $0.22''$ at 25 GHz. This is close to, but smaller than, the FWHM of the synthesized beam ($0.39'' \times 0.28''$) listed in Table 2.1. Such a result is as per expectation, since several factors beyond the scope of discussion in this thesis will work to make the actual angular resolution somewhat higher than the idealized calculation presented here.

Table 2.1: Parameters for 25 GHz VLA observations

Parameter	Value
Date	2016 July 31
Configuration	B
R.A. of field center (J2000)	$19^{\rm h}\ 23^{\rm m}\ 43\overset{\rm s}{.}90$
Decl. of field center (J2000)	$14^\circ\ 30'\ 29\overset{''}{.}00$
Total Bandwidth (MHz)	8.0
Channel spacing (kHz)	7.8125
Approx. time on source (min)	13.5
Rest frequency (GHz)	24.95908 & 25.01812
FWHM of synthesized beam	$0.39'' \times 0.28''$
Line rms noise (mJy/beam)	12

In order to determine whether the observed 25 GHz CH_3OH masers had any counterparts at 36 GHz and 44 GHz, the same field was also observed at a rest frequency of 36.16929 GHz on 2016 August 7 and at a rest frequency of 44.069488 GHz on 2016 August 5. The FWHM of the synthesized beam is $0.37'' \times 0.20''$ for the 36 GHz observations, and $0.29'' \times 0.16''$ for the 44 GHz observations.

Before any analysis can be done with VLA data, it must be edited, calibrated, and imaged. The editing and calibration of the data were done by E. Momjian (NRAO scientist and collaborator on the project), and the data were then imaged by A. P. Sarma. The final images were comprised of two data cubes, one for the 24.959 GHz data and the other for the 25.018 GHz data and it was with these images that I began work for my thesis project.

The search for masers in the images used the NRAO Astronomical Image Processing System (AIPS). This software is designed for interactive analysis of interferometer observations. The AIPS task TVSAD was used to search for masers in the data cube. To use this task, the user first defines a minimum intensity. TVSAD then steps through each data cube, channel by channel, identifying regions with intensity above the defined limit. Ideally, the limit should be defined at a reasonable level above the noise to avoid false detections. Here the limit was set to 100 mJy beam^{-1}, about a factor of 8 above the rms noise level of 12 mJy beam^{-1}. The results of TVSAD are written to an extension file named MF that is attached to the data cube. Using the AIPS task MFPRT, this information is written into a text file for later use. With the locations determined by the TVSAD task, spectra can be plotted using another AIPS task known as ISPEC. When this was done, only one maser was detected in each of the two 25 GHz data cubes, and the maser location is the same for the 24.959 GHz and 25.018 GHz masers. The image cubes for the 36 GHz and 44 GHz were prepared in the same manner by E. Momjian and A. P. Sarma, and the ISPEC task was then used to plot spectra at the same position as the 25 GHz masers. A comparison of the spectra at different bands can help determine if any additional emission present is coincident with the 25 GHz maser.

The next step was to fit Gaussian profiles to the 24.959 GHz and 25.018 GHz data. This was done using the AIPS task XGAUS. XGAUS works only on data cubes with frequency (or velocity) as the first axis so the AIPS task TRANS was used to convert the order of the data cubes from '123' to '312' (i.e., from R.A.–Decl.–velocity to velocity–R.A.–Decl.). While XGAUS is capable of fitting multiple Gaussians to the spectra, only one was required since both the 24.959 GHz and 25.018 GHz masers have a simple structure. The fit was declared satisfactory by a visual examination of the residuals and by noting how well it overlaid the observed profile.

2.2 Archival Data

The archival data described in this thesis were obtained from the site `maserdb.net` (Ladeyschikov et al. 2019). Figure 2.1 shows a view of the top part of the landing page for this website. Clicking on `Maser Transitions` (marked by the red oval in Figure 2.1) takes the user to a page specifying the transitions of masers included in the database; the default view is for H_2O masers. Upon selecting the maser type listed in the box enclosed by the rounded rectangle at the top of this page, the user is presented with a listing of the published papers corresponding to the specified maser transitions; a partial view of this page is shown in Figure 2.2. The two transitions at 24.959 and 25.018 GHz for which data were obtained for this thesis are highlighted by the dark red rectangle. A total of 5 papers are listed for the 24.959 GHz transition and 6 papers for the 25.018 GHz transition. Data were taken from four of the five papers listed for the 24.959 GHz transition and four of the six papers for the 25.018 GHz transition; the other papers contained only single dish observations and their sources had been re-observed with interferometers in the papers that were used. Clicking on each of these references takes the user to a page from which the paper is linked and the data in the paper can be obtained as csv files. These six csv data files were downloaded from the database and aggregated into one Excel file keeping the relevant information for later comparison. The collected data included a source identification name, Right Ascension (R.A.) and Declination (Decl.) coordinates (in epoch J2000), the peak intensity (in Jy beam^{-1}), the velocity at the peak of the line (center velocity or $v_{\rm LSR}$), the Full Width at Half Maximum (FWHM) linewidth if available, the frequency of the transition (written as K1 for 24.959 GHz, and K2 for 25.018 GHz), and the reference from which these data were obtained. The contents of this consolidated Excel file are presented in Table 3.2.

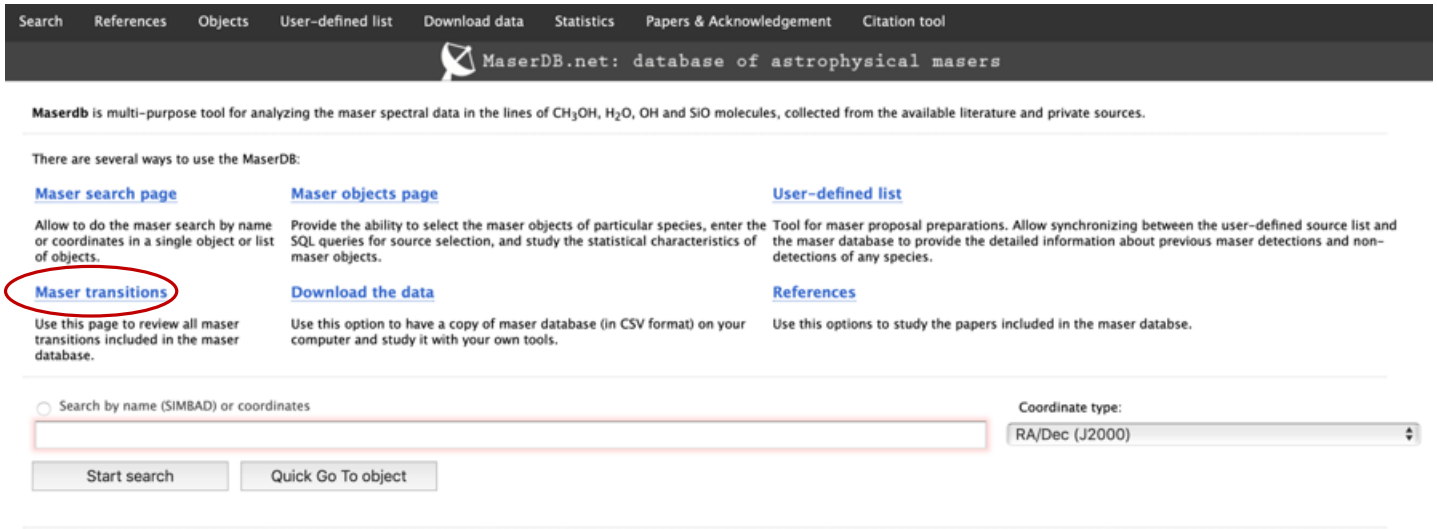

Figure 2.1: A view of the top part of the landing page for the website `maserdb.net` that was used to search for the archival data. The dark red oval has been inserted to highlight the link to follow to get to the list of maser transitions.

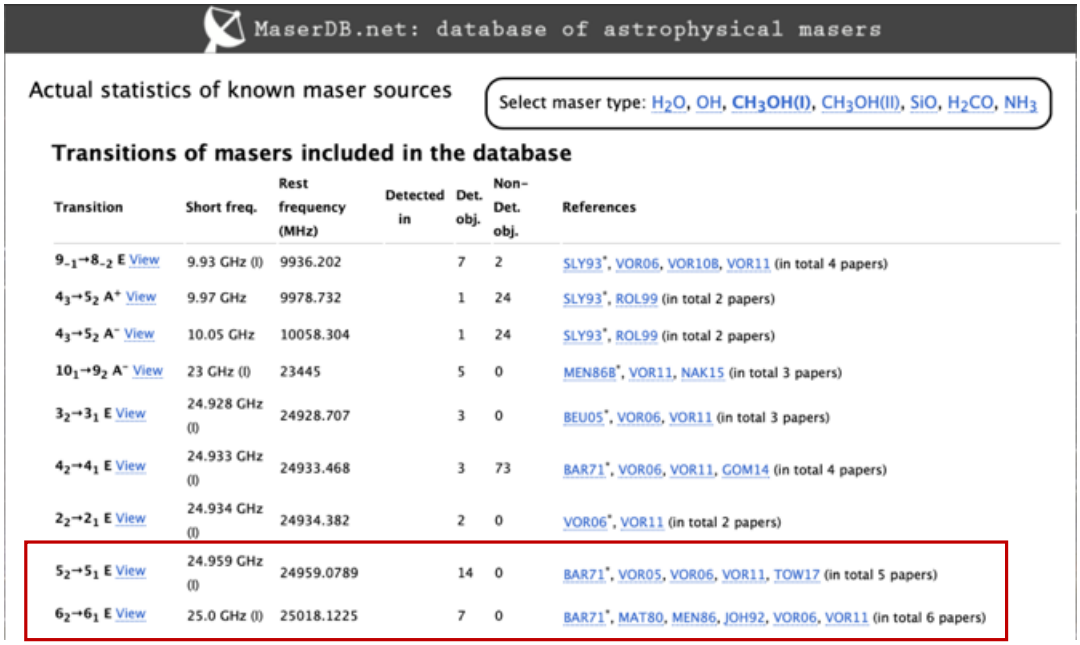

MaserDB.net: database of astrophysical masers

Actual statistics of known maser sources

Select maser type: H_2O, OH, $CH_3OH(I)$, $CH_3OH(II)$, SiO, H_2CO, NH_3

Transitions of masers included in the database

Transition	Short freq.	Rest frequency (MHz)	Detected in	Det. obj.	Non-Det. obj.	References
$9_{-1}\rightarrow8_{-2}$ E View	9.93 GHz (I)	9936.202		7	2	SLY93*, VOR06, VOR10B, VOR11 (in total 4 papers)
$4_3\rightarrow5_2$ A^+ View	9.97 GHz	9978.732		1	24	SLY93*, ROL99 (in total 2 papers)
$4_3\rightarrow5_2$ A^- View	10.05 GHz	10058.304		1	24	SLY93*, ROL99 (in total 2 papers)
$10_1\rightarrow9_2$ A^- View	23 GHz (I)	23445		5	0	MEN86B*, VOR11, NAK15 (in total 3 papers)
$3_2\rightarrow3_1$ E View	24.928 GHz (I)	24928.707		3	0	BEU05*, VOR06, VOR11 (in total 3 papers)
$4_2\rightarrow4_1$ E View	24.933 GHz (I)	24933.468		3	73	BAR71*, VOR06, VOR11, GOM14 (in total 4 papers)
$2_2\rightarrow2_1$ E View	24.934 GHz (I)	24934.382		2	0	VOR06*, VOR11 (in total 2 papers)
$5_2\rightarrow5_1$ E View	24.959 GHz (I)	24959.0789		14	0	BAR71*, VOR05, VOR06, VOR11, TOW17 (in total 5 papers)
$6_2\rightarrow6_1$ E View	25.0 GHz (I)	25018.1225		7	0	BAR71*, MAT80, MEN86, JOH92, VOR06, VOR11 (in total 6 papers)

Figure 2.2: A view of the maserdb.net page listing the Class I CH_3OH maser transitions and their references. The transitions discussed in this thesis are highlighted by the dark red rectangle.

CHAPTER 3

Results

This thesis presents observations of the 25 GHz CH_3OH masers toward the high mass star forming region W51A. Chapter 3 presents the results of the observations. The masers observed at 24.959 and 25.018 GHz are presented in Section 3.1. Spectral profiles of the methanol emission at 36 GHz and 44 GHz at the position of the 25 GHz masers are also presented in this section. Archival data on 24.959 and 25.018 GHz CH_3OH masers in high mass star forming regions are presented in Section 3.2.

3.1 The 25 GHz methanol masers in W51A

Figure 3.1 shows the Class I CH_3OH maser profile at 24.959 GHz toward W51A. Spectral profiles of intensity *vs.* velocity such as these are characterized by three quantities: the peak intensity of the profile, the velocity at line center (henceforth referred to as the center velocity), and the linewidth. For Galactic observations, it is customary to measure the center velocity with respect to the Local Standard of Rest (LSR), a hypothetical point in space that is moving in a perfectly circular orbit around the Galactic center at the Sun's galactocentric distance. The linewidth is the spread in velocity of the spectral lines measured at half the maximum intensity, and is usually referred to as the Full Width at Half Maximum (FWHM). These three quantities can be obtained by eyeballing the observed profile but it is considered better practice to figure them out by fitting a Gaussian, $G(v)$, to the observed spectral

profile, with

$$G(v) = I_0 * \exp\left[-\frac{(v - v_{\rm LSR})^2}{2\sigma^2}\right] \tag{3.1}$$

where I_0 is the peak intensity, $v_{\rm LSR}$ is the center velocity, and the dispersion σ is related to the FWHM linewidth Δv by

$$\sigma = \frac{\Delta v}{\sqrt{8 \ln 2}} \tag{3.2}$$

The peak intensity, center velocity ($v_{\rm LSR}$), and FWHM linewidth (Δv) obtained from the Gaussian fit (equation 3.1) to the observed spectral profile are listed in Table 3.1. The position of this maser in Right Ascension (R.A.) and Declination (Decl.) is also listed in this table. The peak intensity of this maser is 213.14 mJy beam^{-1}, and even though this is an intrinsically low value, we have an unambiguous detection of the signal at a level of 18σ above the rms noise level of 12 mJy beam^{-1}. How we know this is a maser and not a thermal line is discussed in Section 4.1. An immediate clue to its maser nature is the very narrow linewidth of 0.32 km s^{-1}. The center velocity of this maser is 58.83 km s^{-1}.

Table 3.1: Fitted parameters of the 25 GHz Class I CH_3OH masers

Frequency (GHz)	R.A. (J2000)	Decl. (J2000)	Peak Intensity (mJy beam^{-1})	Center Velocity (km s^{-1})	Velocity Width (km s^{-1})
24.959	19 23 43.77	14 30 15.64	213.14 ± 9.18	58.83 ± 0.01	0.32 ± 0.02
25.018	19 23 43.77	14 30 15.64	365.34 ± 8.72	58.77 ± 0.01	0.34 ± 0.01

Note: R.A. is in $^{\rm h}$ $^{\rm m}$ $^{\rm s}$ (hr min sec), and Decl. in $^\circ$ $'$ $''$. The velocity width is at FWHM (Full Width at Half Maximum).

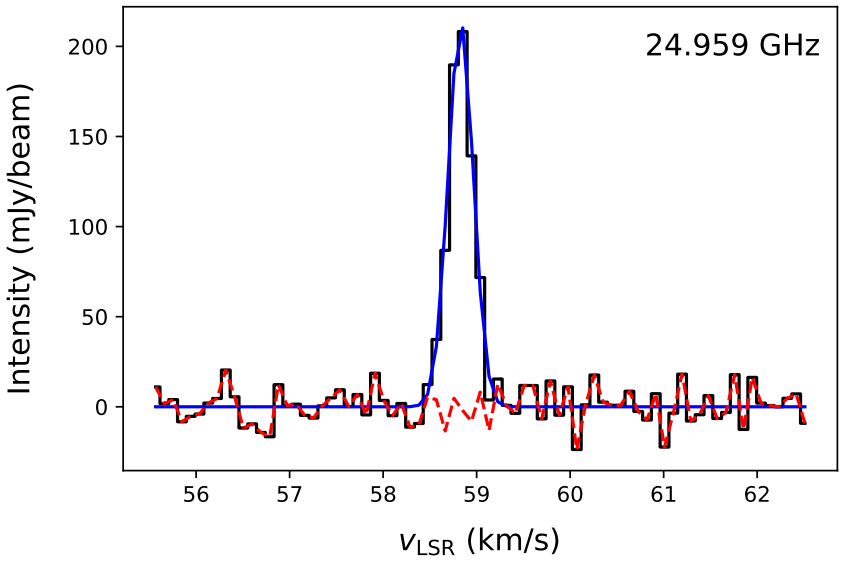

Figure 3.1: Spectral profile of the Class I CH_3OH maser toward W51A at 24.959 GHz. The profile is toward the position R.A. (J2000) = RA $19^h\ 23^m\ 43\overset{s}{.}77$ and Decl. (J2000) = $14°30'15\overset{''}{.}64$. The black histogram-like profile shows the observed data. The blue line shows the Gaussian profile fitted to the data, and the dashed red line shows the residuals.

Figure 3.2 shows the Class I CH_3OH maser profile at 25.018 GHz toward the same position as the 24.959 GHz maser in W51A. The peak intensity, center velocity (v_{LSR}), and FWHM linewidth (Δv) obtained from the Gaussian fit to the observed spectral profile, as well as the position in R.A. and Decl., are listed in Table 3.1. With a peak intensity of 365.34 mJy beam^{-1}, this maser is a factor of 1.7 higher in intensity than the 24.959 GHz maser. This maser too has a narrow linewidth, almost the same as the 24.959 GHz maser. The center velocity is 58.77 km s^{-1}, close to the 58.83 km s^{-1} velocity of the 24.959 GHz maser.

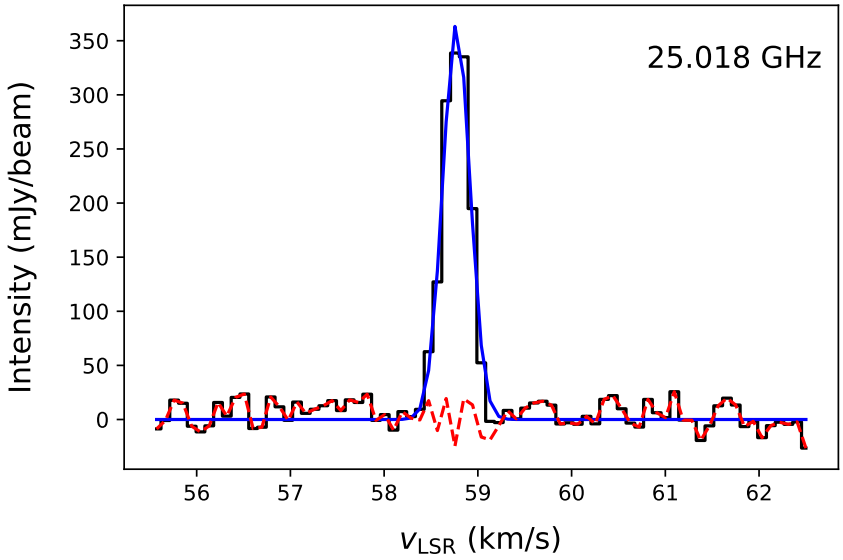

Figure 3.2: Spectral profile of the Class I CH_3OH maser toward W51A at 25.018 GHz. The profile is toward the same position listed in the caption to Figure 3.1. The black histogram-like profile shows the observed data. The blue line shows the Gaussian profile fitted to the data, and the dashed red line shows the residuals.

Figure 3.3 shows the observed spectral profile at 36 GHz toward W51A at the same position as the 25 GHz masers. There is no obvious maser profile seen at this frequency. To the eye, there is a hint of a maser-like protrusion centered at a velocity to the left of the 59 km s^{-1} mark. However, the rms noise at 36 GHz is 23 mJy $beam^{-1}$, about a factor of 2 higher than at 25 GHz. So the 40 mJy $beam^{-1}$ feature to the left of 59 km s^{-1} in the 36 GHz profile is barely 1.5σ above the rms noise level. The broad spectral profile suggests that there is some thermal emission toward this position at 36 GHz, but there appears to be no significant maser emission. To highlight the absence of maser emission near the center velocities of the 25 GHz masers, the 36 GHz profile was scaled by a factor of 2, the ratio of the rms in the 36 GHz image to the rms in the 25 GHz images. This scaled version of the 36 GHz profile was then plotted with the observed 24.959 GHz profile in Figure 3.4. From this figure, it is clear that there is no maser emission at 36 GHz near the 58.83 km s^{-1} center velocity of the 24.959 GHz maser.

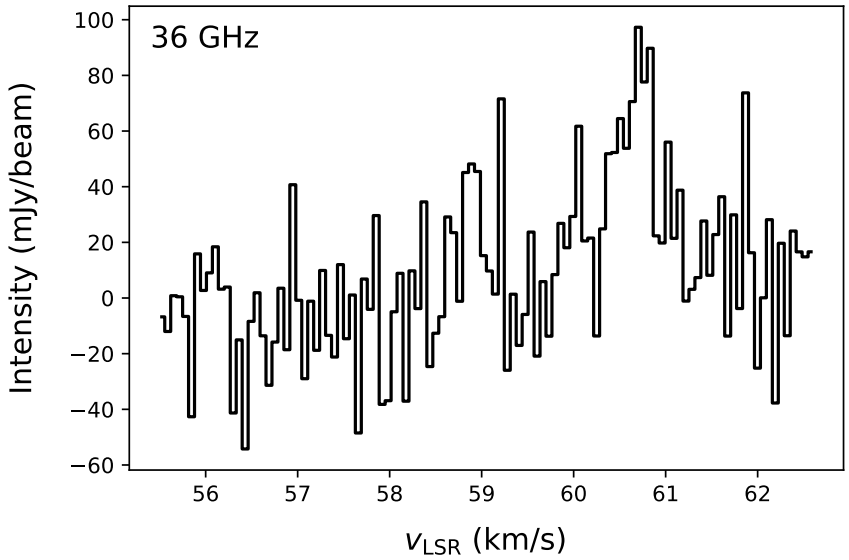

Figure 3.3: Spectral profile at 36 GHz toward the position of the 25 GHz Class I CH_3OH masers in W51A.

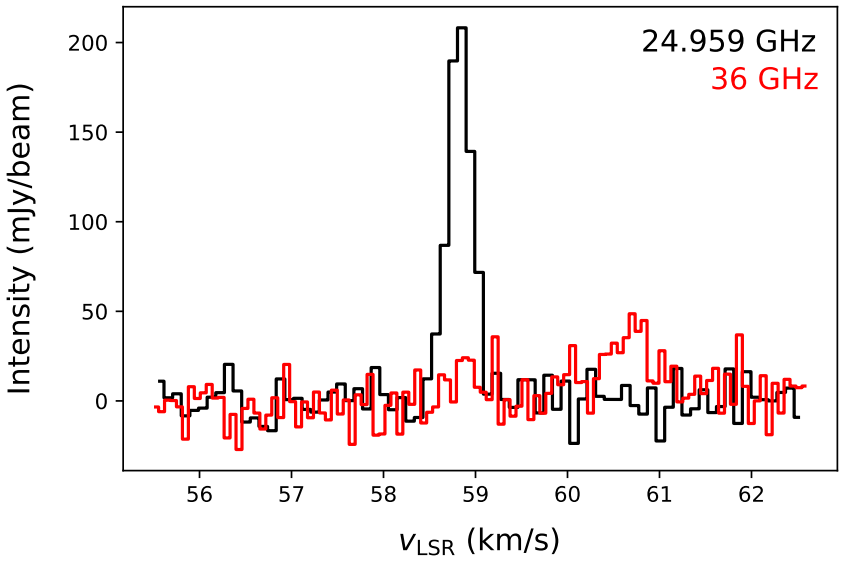

Figure 3.4: Spectral profile of the 24.959 GHz Class I CH_3OH maser toward W51A (black) together with the profile at 36 GHz (red) toward the same position. The 36 GHz profile has been scaled down by a factor of 2 (the ratio of the rms in the 36 GHz image cube to the rms in the 25 GHz image cube) to demonstrate that there is no 36 GHz emission within the velocity range of the 25 GHz emission.

Figure 3.5 shows the spectral profile at 44 GHz toward W51A at the same position as the 25 GHz masers. This profile shows significant high intensity emission peaking at over 800 mJy beam^{-1} which could be blended masers or broad thermal emission, or a mixture of both. However, this emission is shifted in velocity from that of the 25 GHz masers. To highlight this, a scaled-down version of the 44 GHz profile was plotted with the spectral profile of the 24.959 GHz maser, as shown in Figure 3.6. The 44 GHz profile was scaled by a factor of 5, the ratio of the rms in the 44 GHz image to the rms in the 25 GHz image. Figure 3.6 demonstrates clearly that there is no 44 GHz emission coincident with the 58.83 km s^{-1} center velocity of the 24.959 GHz maser.

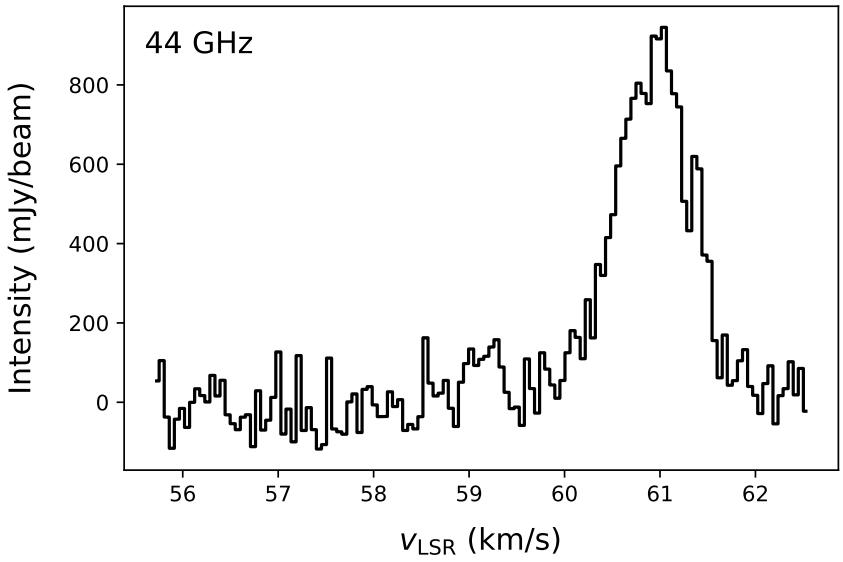

Figure 3.5: Spectral profile at 44 GHz toward the position of the 25 GHz Class I CH_3OH masers in W51A.

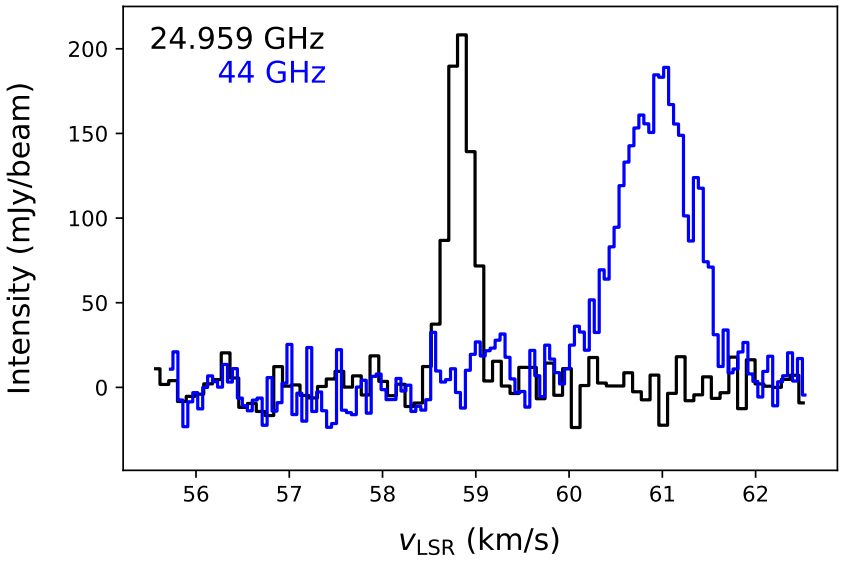

Figure 3.6: Spectral profile of the 24.959 GHz Class I CH_3OH maser toward W51A (black) together with the profile at 44 GHz (blue) toward the same position. The 44 GHz spectral profile has been scaled down by a factor of 5 (the ratio of the rms in the 44 GHz image cube to the rms in the 25 GHz image cube) to demonstrate that there is no 44 GHz emission within the velocity range of the 25 GHz emission. The full vertical height of the 44 GHz emission can be seen in Figure 3.5.

3.2 25 GHz methanol masers in star forming regions

In order to place the 25 GHz masers observed toward W51A in context, archival data were obtained from the site `maserdb.net` (Ladeyschikov et al. 2019). Data were obtained for both the transitions observed for this thesis, 24.959 and 25.018 GHz. The `maserdb.net` site lists 20 objects in which such CH_3OH masers have been detected. It is worth noting that the reference here is to objects, not individual masers. Each site can have multiple CH_3OH masers at either or both frequencies. The total number of CH_3OH masers in these archival data is 88, and they are listed in Table 3.2. The first column in this table gives the source name. The position of the source, its Right Ascension (R.A.) and Declination (Decl.) in epoch J2000 are listed in the second and third columns respectively. The peak intensity (in Jy beam^{-1}), velocity at line center (labeled as center velocity, in km s^{-1}), and the Full Width at Half Maximum (FWHM) linewidth (in km s^{-1}) are listed in the fourth, fifth, and sixth columns of Table 3.2. The seventh column lists the frequency at which the maser was observed; code K1 in this column means that the maser was observed at 24.959 GHz, and code K2 in this column means that the maser was observed at 25.018 GHz. The reference from which the data were obtained for the listing on `maserdb.net` is given in the last column. Note that, of the 15 masers listed in Table 3.2 that were observed at 25.018 GHz toward Orion-KL, 12 were also observed at 24.959 GHz but their line parameters are not listed in this table. Another maser was observed at 24.959 GHz but not at 25.018 GHz in Orion-KL, but its line parameters are not listed in Table 3.2.

The intensities of the 25 GHz masers listed in Table 3.2 show a wide range, from values as high as 100 Jy beam^{-1} down to a mere 0.010 Jy beam^{-1}. The FWHM line widths, wherever available, can be as narrow as 0.2 km s^{-1}, but the line widths measured by Menten et al. (1986), reference (1) listed in the table, are broader, in the range 0.5 - 0.8 km s^{-1}. However, the Menten et al. (1986) observations were carried

out with a single dish telescope so they could be suffering from velocity blending due to positional coincidences. More details of these masers are discussed in Section 4.2.

Table 3.2: Archival Data of 25 GHz Observations

Source Name	R.A. (J2000)	Decl. (J2000)	Peak Intensity (Jy beam^{-1})	Center Velocity (km s^{-1})	FWHM (km s^{-1})	Line	Ref.
W33	18 14 11.10	-17 55 57.40	5.2	33.2	0.5	K2	(1)
W51 Met1	19 23 43.90	14 29 25.40	1.0	53.8	0.7	K2	(1)
W51 Met2	19 23 46.50	14 29 40.60	2.9	56.8	0.7	K2	(1)
W51 Met3	19 23 45.20	14 29 45.50	0.4	59.3	0.7	K2	(1)
W51 Met4	19 23 43.20	14 31 34.40	1.7	64.5	0.7	K2	(1)
W51 Met5	19 23 38.20	14 30 5.00	0.7	66.7	0.8	K2	(1)
DR21 West	20 38 54.60	42 19 23.50	13.8	-2.6	0.5	K2	(1)
W31 1	18 10 29.00	-19 55 43.60	1.6	-6.0	0.6	K2	(1)
W31 2	18 10 29.10	-19 55 42.60	1.8	-8.0	0.8	K2	(1)
Orion-KL 1	5 35 14.23	-5 22 15.58	23.4	9.9	$\cdots$	K2	(2)

Continued on next page

Table 3.2: *Continued from previous page*

Source Name	R.A. (J2000)	Decl. (J2000)	Peak Intensity (Jy beam^{-1})	Center Velocity (km s^{-1})	FWHM (km s^{-1})	Line	Ref.
Orion-KL 2	5 35 14.42	-5 22 36.39	2.8	9.17	···	K2	(2)
Orion-KL 3	5 35 13.66	-5 22 25.02	4.6	9.02	···	K2	(2)
Orion-KL 4	5 35 13.90	-5 22 33.90	5.3	9.02	···	K2	(2)
Orion-KL 5	5 35 14.22	-5 22 25.92	28.7	8.73	···	K2	(2)
Orion-KL 6	5 35 13.87	-5 22 41.91	6.3	8.58	···	K2	(2)
Orion-KL 7	5 35 13.72	-5 22 25.75	56.9	8.29	···	K2	(2)
Orion-KL 8	5 35 14.21	-5 22 41.20	12.7	8.00	···	K2	(2)
Orion-KL 9	5 35 13.98	-5 22 36.63	5.2	8.00	···	K2	(2)
Orion-KL 10	5 35 15.24	-5 22 45.72	22.5	8.00	···	K2	(2)
Orion-KL 11	5 35 13.62	-5 22 24.06	100.8	8.00	···	K2	(2)

Continued on next page

Table 3.2: *Continued from previous page*

Source Name	R.A. (J2000)	Decl. (J2000)	Peak Intensity (Jy beam^{-1})	Center Velocity (km s^{-1})	FWHM (km s^{-1})	Line	Ref.
Orion-KL 12	5 35 13.93	-5 22 29.91	7.5	7.42	···	K2	(2)
Orion-KL 13	5 35 14.99	-5 22 45.59	37.7	7.42	···	K2	(2)
Orion-KL 14	5 35 14.72	-5 22 44.98	6.3	7.13	···	K2	(2)
Orion-KL 15	5 35 15.12	-5 22 47.17	7.7	6.96	···	K2	(2)
OMC-1 1	5 35 14.87	-5 22 44.00	35.0	7.34	···	K1	(3)
OMC-1 2	5 35 14.83	-5 22 42.80	48.0	7.58	···	K1	(3)
OMC-1 3	5 35 14.33	-5 22 36.50	68.0	7.95	···	K1	(3)
OMC-1 4	5 35 14.02	-5 22 30.90	89.0	8.28	···	K1	(3)
OMC-1 5	5 35 14.02	-5 22 31.80	45.0	8.75	···	K1	(3)
OMC-1 6	5 35 14.19	-5 22 14.00	14.0	9.92	···	K1	(3)

Continued on next page

Table 3.2: *Continued from previous page*

Source Name	R.A. (J2000)	Decl. (J2000)	Peak Intensity (Jy beam^{-1})	Center Velocity (km s^{-1})	FWHM (km s^{-1})	Line	Ref.
IRAS 16547-4247 1	16 58 16.44	-42 52 26.40	0.2	-31.69	···	K1	(4)
IRAS 16547-4247 2	16 58 16.46	-42 52 25.90	5.2	-31.62	···	K1	(4)
IRAS 16547-4247 3	16 58 16.46	-42 52 25.90	0.6	-31.63	···	K1	(4)
IRAS 16547-4247 4	16 58 16.46	-42 52 25.90	8.3	-31.72	···	K1	(4)
IRAS 16547-4247 5	16 58 16.46	-42 52 25.90	0.6	-31.80	···	K1	(4)
IRAS 16547-4247 6	16 58 16.46	-42 52 25.70	6.4	-31.68	···	K1	(4)
IRAS 16547-4247 7	16 58 16.46	-42 52 25.70	0.5	-31.82	···	K1	(4)
IRAS 16547-4247 8	16 58 16.58	-42 52 25.50	0.4	-31.24	···	K1	(4)
IRAS 16547-4247 9	16 58 16.46	-42 52 25.76	7.3	-31.70	···	K2	(4)
IRAS 16547-4247 10	16 58 16.46	-42 52 25.76	0.5	-31.89	···	K2	(4)

Continued on next page

Table 3.2: *Continued from previous page*

Source Name	R.A. (J2000)	Decl. (J2000)	Peak Intensity (Jy beam^{-1})	Center Velocity (km s^{-1})	FWHM (km s^{-1})	Line	Ref.
IRAS 16547-4247 11	16 58 16.59	-42 52 25.32	0.6	-31.23	···	K2	(4)
IRAS 16547-4247 12	16 58 16.45	-42 52 25.70	6.8	-31.65	···	K2	(4)
IRAS 16547-4247 13	16 58 16.45	-42 52 25.70	0.8	-31.80	···	K2	(4)
IRAS 16547-4247 14	16 58 16.58	-42 52 25.25	0.5	-31.20	···	K2	(4)
G357.97-0.16 1	17 41 19.10	-30 44 58.10	0.37	-5.63	0.33	K1	(5)
G357.97-0.16 2	17 41 19.10	-30 44 58.10	0.74	-5.27	0.24	K1	(5)
G357.97-0.16 3	17 41 19.10	-30 44 58.10	4.60	-4.74	0.39	K1	(5)
G357.97-0.16 4	17 41 19.10	-30 44 58.10	0.31	-5.67	0.34	K2	(5)
G357.97-0.16 5	17 41 19.10	-30 44 58.10	0.53	-5.30	0.27	K2	(5)
G357.97-0.16 6	17 41 19.10	-30 44 58.10	3.78	-4.79	0.433	K2	(5)

Continued on next page

Table 3.2: *Continued from previous page*

Source Name	R.A. (J2000)	Decl. (J2000)	Peak Intensity (Jy beam^{-1})	Center Velocity (km s^{-1})	FWHM (km s^{-1})	Line	Ref.
G08.67-0.35 a	18 6 18.60	-21 37 22.72	0.010	38.2	···	K1	(6)
G08.67-0.35 b	18 6 18.88	-21 37 18.90	0.013	38.2	···	K1	(6)
G08.67-0.35 c	18 6 19.00	-21 37 26.34	0.044	35.0	···	K1	(6)
G08.67-0.35 d	18 6 19.02	-21 37 32.15	0.130	36.2	···	K1	(6)
G08.67-0.35 e	18 6 19.04	-21 37 40.18	0.099	33.4	···	K1	(6)
G08.67-0.35 f	18 6 19.10	-21 37 27.05	0.023	36.2	···	K1	(6)
G08.67-0.35 g	18 6 19.16	-21 37 23.95	0.028	35.4	···	K1	(6)
G08.67-0.35 h	18 6 19.17	-21 37 25.43	0.791	35.8	···	K1	(6)
G08.67-0.35 i	18 6 19.54	-21 37 14.60	0.027	36.6	···	K1	(6)
G10.29-0.13 a	18 8 45.80	-20 5 43.85	0.288	14.6	···	K1	(6)

Continued on next page

Table 3.2: *Continued from previous page*

Source Name	R.A. (J2000)	Decl. (J2000)	Peak Intensity (Jy beam^{-1})	Center Velocity (km s^{-1})	FWHM (km s^{-1})	Line	Ref.
G10.29-0.13 b	18 8 52.42	-20 6 3.20	0.097	15.4	···	K1	(6)
G10.34-0.14 a	18 8 59.64	-20 3 32.66	2.76	14.8	···	K1	(6)
G10.34-0.14 b	18 8 59.96	-20 3 36.68	0.041	12.8	···	K1	(6)
G10.34-0.14 c	18 9 0.74	-20 3 48.30	0.036	11.6	···	K1	(6)
G11.92-0.61 a	18 13 57.72	-18 54 25.84	0.511	34.0	···	K1	(6)
G11.92-0.61 b	18 13 57.74	-18 54 26.64	0.035	35.2	···	K1	(6)
G11.92-0.61 c	18 13 57.82	-18 54 8.30	0.018	36.4	···	K1	(6)
G11.92-0.61 d	18 13 58.11	-18 54 20.21	0.054	36.8	···	K1	(6)
G11.92-0.61 e	18 13 58.72	-18 54 15.57	0.018	36.8	···	K1	(6)
G12.68-0.18 a	18 13 54.73	-18 1 46.41	0.033	56.0	···	K1	(6)

Continued on next page

Table 3.2: *Continued from previous page*

Source Name	R.A. (J2000)	Decl. (J2000)	Peak Intensity (Jy beam^{-1})	Center Velocity (km s^{-1})	FWHM (km s^{-1})	Line	Ref.
G12.68-0.18 b	18 13 54.76	-18 1 46.54	0.018	52.4	···	K1	(6)
G12.91-0.03 a	18 13 47.36	-17 45 40.46	0.023	55.0	···	K1	(6)
G12.91-0.03 b	18 13 48.27	-17 45 38.36	0.059	57.8	···	K1	(6)
G14.33-0.64 a	18 18 54.30	-16 47 53.06	0.099	21.6	···	K1	(6)
G14.33-0.64 b	18 18 54.52	-16 47 44.86	0.400	20.4	···	K1	(6)
G14.33-0.64 c	18 18 54.68	-16 47 44.54	0.041	22.4	···	K1	(6)
G14.33-0.64 d	18 18 54.77	-16 47 49.84	0.058	22.8	···	K1	(6)
G14.63-0.58 a	18 19 15.46	-16 29 53.18	0.019	19.4	···	K1	(6)
G16.59-0.05 a	18 21 9.10	-14 31 48.69	0.036	58.6	···	K1	(6)
G16.59-0.05 b	18 21 9.13	-14 31 49.86	0.320	61.4	···	K1	(6)

Continued on next page

Table 3.2: *Continued from previous page*

Source Name	R.A. (J2000)	Decl. (J2000)	Peak Intensity (Jy beam^{-1})	Center Velocity (km s^{-1})	FWHM (km s^{-1})	Line	Ref.
G18.67+0.03 a	18 24 53.78	-12 39 21.01	0.012	78.2	···	K1	(6)
G19.36-0.03 a	18 26 25.60	-12 3 47.44	0.130	26.0	···	K1	(6)
G19.36-0.03 b	18 26 25.77	-12 3 51.11	0.091	26.4	···	K1	(6)
G19.36-0.03 c	18 26 25.80	-12 3 53.43	0.046	27.6	···	K1	(6)
G19.36-0.03 d	18 26 25.96	-12 3 59.55	6.39	26.4	···	K1	(6)
G22.04+0.22 a	18 30 34.60	-9 34 48.09	7.65	51.8	···	K1	(6)
G22.04+0.22 b	18 30 34.68	-9 34 46.91	0.200	50.2	···	K1	(6)
G22.04+0.22 c	18 30 34.73	-9 34 53.56	0.342	50.2	···	K1	(6)

Note: K1 = 24.959 GHz; K2 = 25.018 GHz

References: (1) Menten et al. (1986); (2) Johnston et al. (1992); (3) Voronkov et al. (2005); (4) Voronkov et al. (2006); (5) Voronkov et al. (2011); (6) Towner et al. (2017).

CHAPTER 4

Discussion

The observations carried out for this thesis have revealed a Class I CH_3OH maser at 24.959 GHz toward the high mass star forming region W51A. A Class I CH_3OH maser at 25.018 GHz is coincident in position and velocity extent with the 24.959 GHz maser. These two masers, together with additional 36 GHz and 44 GHz observations toward the position of the 25 GHz masers, are discussed in Section 4.1. The observed masers are compared to the database of the known 25 GHz maser population in Section 4.2, whereas Section 4.3 discusses other known maser species in the region. Finally, the characteristics of the maser region are discussed in Section 4.4.

4.1 The 25 GHz methanol masers in W51A

As described in Section 3.1, only one maser was detected toward W51A at 24.959 GHz. Likewise, only one maser was detected at 25.018 GHz. The masers are spatially coincident, but their peak intensities differ. The peak intensity of the 24.959 GHz maser is 213 mJy beam^{-1}, and the peak intensity of the 25.018 GHz maser is 365 mJy beam^{-1}, about 1.7 times greater. The center velocities of the two masers differ by only 0.06 km s^{-1}, which implies that they have the same center velocity since this difference is within the channel spacing of the observations. To see this, one would need to refer to Table 2.1, where the channel spacing is listed as

7.8125 kHz. To convert this to velocity units, we can use

$$\frac{\Delta f}{f} = \frac{\Delta v}{c} \tag{4.1}$$

which is adequate for Galactic work; for extragalactic observations we would need to use a relativistic correction. In equation 4.1, f is the rest frequency, c is the speed of light, Δf is the channel spacing in frequency units, and Δv is the channel spacing in velocity units. Substituting appropriate values, we obtain

$$\frac{7.8125 \times 10^3 \text{ Hz}}{25 \times 10^9 \text{ Hz}} = \frac{\Delta v}{3 \times 10^5 \text{ km s}^{-1}}$$

or $\Delta v = 0.09$ km s^{-1}. Since the difference between the center velocities of the 24.959 GHz and 25.018 GHz masers is 0.06 km s^{-1}, less than the channel spacing of 0.09 km s^{-1}, we conclude that these masers have roughly the same center velocity. Since the masers are spatially coincident and coincide in velocity too, we conclude that they arise in the same clump of velocity-coherent gas.

How do we know these objects are masers? The observed narrow linewidths of the spectral profile are one way to tell. The 24.959 GHz maser has a linewidth of 0.32 km s^{-1}, and the 25.018 GHz maser has a linewidth of 0.34 km s^{-1} (Table 3.1). They also appear to be compact sources, as seen in the contour plots of the peak maser channel in Figure 4.1 and 4.2. A more reliable way to tell they are masers, though, is by estimating their brightness temperatures.

The concept of brightness temperature comes to us from an approximation for the Planck law, the well-known equation of physics that describes the intensity radiated by a black body. This approximation is valid when $h\nu \ll kT$, which is always true at radio frequencies. Here, h is the Planck constant, ν is the frequency, k is the Boltzmann constant, and T is the temperature of the radiating black body. Whenever $h\nu \ll kT$, we can approximate the Planck law with the Rayleigh-Jeans

law, for which the intensity or brightness B_ν emitted at a particular frequency ν is given by:

$$B_\nu \simeq \frac{2\nu^2 k T_\mathrm{b}}{c^2} \tag{4.2}$$

Rearranging, we obtain that

$$T_\mathrm{b} \simeq \frac{c^2\, B_\nu}{2\nu^2 k} \tag{4.3}$$

The quantity T_b is called the brightness temperature; T_b may be formally defined as the temperature at which a blackbody has the same intensity as the observed line (at that frequency). That is, T_b is the equivalent temperature that a black body would need to have to be as bright as what is observed, which also implies that T_b may have no connection to an actual physical temperature in the source.

Equation (4.3) needs to be expressed in terms of quantities measured with the VLA to be of practical use. The following is taken from a note provided by the National Radio Astronomy Observatory (NRAO)[1]. The quantity B_ν in equation (4.3) has SI units of watts m^{-2} Hz^{-1} sr^{-1}. Radio astronomers usually work with the flux density, S_ν, which has units of watts m^{-2} Hz^{-1}. This unit is too large for practical use, so radio astronomers use jansky (Jy), where 1 Jy $\equiv 10^{-26}$ watts m^{-2} Hz^{-1}. Finally, interferometric images obtained with the VLA are usually expressed in brightness units of Jy beam^{-1}, where the beam is a nominal area over which the brightness is defined. Therefore, the quantity B_ν in equation (4.3) can be replaced by S_ν/Ω, where Ω is the beam solid angle. Furthermore

$$\frac{S_\nu}{\Omega} = \frac{S_\nu/\mathrm{beam}}{\Omega/\mathrm{beam}} = \frac{I_\nu}{\Omega/\mathrm{beam}} = I_\nu \left(\frac{\mathrm{beam}}{\Omega}\right) \tag{4.4}$$

where I_ν is in Jy/beam and beam/Ω denotes the conversion of the beam to a solid angle in units of steradian.

[1]The NRAO note is at https://science.nrao.edu/facilities/vla/proposing/TBconv

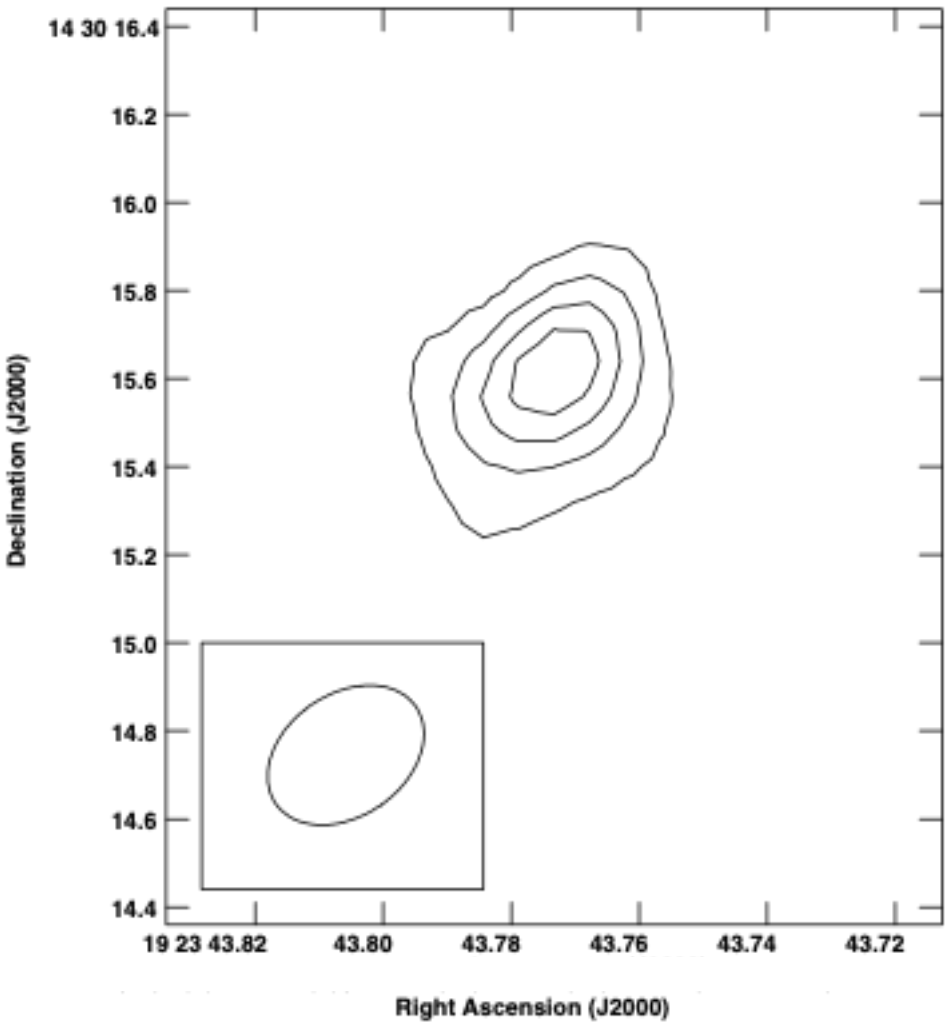

Figure 4.1: Contour image of the peak channel of the 24.959 GHz maser. Contours are at 20%, 40%, 60%, and 80% of the maser peak. The synthesized beam for the observations is shown in the bottom left.

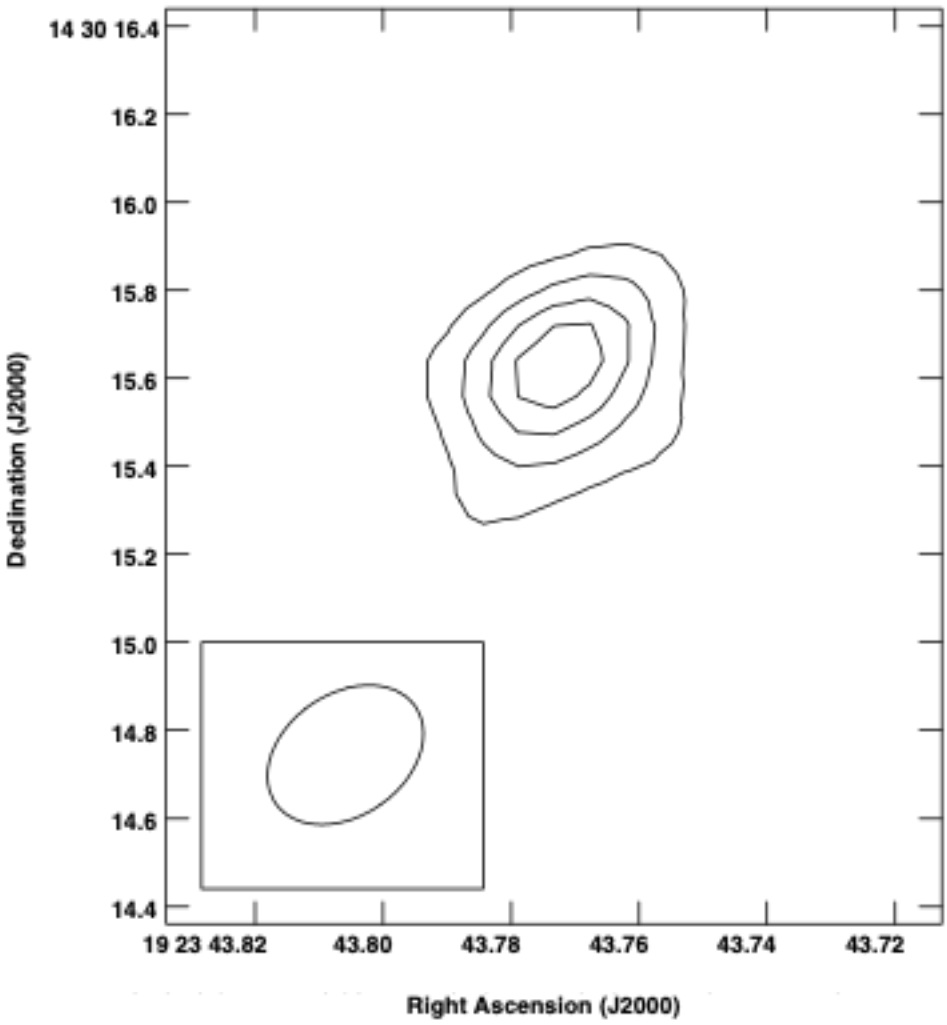

Figure 4.2: Contour image of the peak channel of the 25.018 GHz maser. Contours are at 20%, 40%, 60%, and 80% of the maser peak. The synthesized beam for the observations is shown in the bottom left.

The area of a Gaussian beam such as that used to obtain the VLA images for this thesis is given by

$$\Omega = \frac{\pi\,\theta_{\rm maj}\,\theta_{\rm min}}{4\,\ln 2} \tag{4.5}$$

where $\theta_{\rm maj}$ and $\theta_{\rm min}$ are the half-power beam widths along the major and minor axes of the beam. After substituting equations (4.4) and (4.5), writing all constants to a pre-factor, and converting to units of mJy beam^{-1} for I_ν, arcseconds for $\theta_{\rm maj}$ and $\theta_{\rm min}$, and GHz for ν, equation (4.3) becomes

$$T_b = 1.222 \times 10^3 \left[\frac{I_\nu}{\nu^2\,\theta_{\rm maj}\,\theta_{\rm min}}\right] \tag{4.6}$$

Since the masers appear marginally resolved in Figure 4.1 and 4.2, meaning that the masers are slightly larger than the beam size, the AIPS task JMFIT was used to fit a two-dimensional Gaussian to the maser in its peak channel. This returned, for the 24.959 GHz source, an integrated intensity of 285.38 mJy beam^{-1}, and source sizes of $\theta_{\rm maj} = 0.46''$, $\theta_{\rm min} = 0.34''$. Substituting these values in equation (4.6), we obtain a brightness temperature of 3579 K. Meanwhile, for the 25.018 GHz source, for which JMFIT gives an integrated intensity of 412.33 mJy beam^{-1} and $\theta_{\rm maj} = 0.44''$, $\theta_{\rm min} = 0.31''$, we obtain $T_b = 5901$ K. These temperatures are high enough that we can exclude thermal radiation as the cause of the spectral line. Instead, the spectral profiles observed toward W51 at 25 GHz must be the result of maser emission.

Also of interest is to figure out if these masers are saturated. The concept of saturation is easy to understand if we think about the exponential growth in intensity of the maser as a result of the amplification process that was described in Section 1.1.1. Such an exponential growth cannot continue indefinitely, since it would lead to infinitely high energy for masers that are amplified along a sufficiently long velocity-coherent column of gas. There will come a time when an equilibrium is established between the upper level being populated by population inversion and

depleted by stimulated emission. In this limit, every pumping event results in a maser photon and the maser is said to be saturated. In their analysis of 25 GHz CH_3OH masers in the high mass star forming region OMC-1, Johnston et al. (1992) wrote that a rough estimate for the saturation condition of masers is given by

$$\frac{\Omega k T_b}{4\pi h\nu} A > \Gamma \tag{4.7}$$

where A is the spontaneous transition rate of the maser line (equal to 8.3×10^{-8} s^{-1} for the 25.018 GHz line), $h\nu/k$ is the transition energy of this line (equal to 1.20 K). The quantity $\Omega/4\pi$ is the magnitude of the maser beaming, meaning what fraction of the total solid angle of 4π the maser emission is emitted into; the exact value is not known for individual masers but since masers are known to be highly beamed by the very nature of their creation, $\Omega/4\pi$ is customarily taken to be equal to 0.1. Finally, Γ is the level decay rate which is of order of 3×10^{-4} s^{-1} for the 25.018 GHz transition. Substituting these numbers in equation (4.7), we find that

$$\left(6.9 \times 10^{-9}\right) T_b > 3 \times 10^{-4}$$

implying that $T_b > 4.3 \times 10^4$ K in order for the 25 GHz masers to be saturated. The calculated brightness temperatures of the 25 GHz masers reported in this thesis are less than this limiting condition by a factor of 10, so the masers toward W51A at this position are likely unsaturated. This is also what one would expect given their observed intensities (200-400 mJy beam^{-1}) reported in Table 3.1. Saturated masers tend to have high intensity because every molecule that has been pumped into the upper state is decaying into the lower state if the maser is saturated. Unsaturated masers are predicted to vary as the pump conditions change over time; therefore, future observations have the opportunity to study the potential variability.

4.2 Comparison to the known 25 GHz maser population

The 25 GHz Class I CH_3OH maser is a rarer phenomenon than the better known 44 GHz and 36 GHz Class I CH_3OH masers. The `maserdb.net` website lists 20 objects in which 24.959 and 25.018 GHz masers have been detected; they are listed in Table 3.2. It is worth noting again that the reference here is to objects, not individual masers. Each object can have multiple masers, as is clear from a glimpse at Table 3.2. Nevertheless, this does place 25 GHz masers in the category of rare objects; the same `maserdb.net` website lists 911 objects in which 36 GHz masers have been detected, and 497 objects in which 44 GHz masers have been detected.

A histogram of the masers detected at 24.959 and 25.018 GHz and listed in Table 3.2 is shown in Figure 4.3. There are 88 masers in this list corresponding to the 20 objects in which 25 GHz masers have been observed. The highest intensity maser in this list is toward the high mass star forming region Orion-KL; this maser has an intensity of 100.8 Jy beam^{-1} and was observed at 25.018 GHz. The highest intensity maser at 24.959 GHz was observed toward another high mass star forming region in Orion known as OMC-1; it has an intensity of 89.0 Jy beam^{-1}. The median value of intensities is 0.6 Jy beam^{-1}. Only 14 masers have intensities higher than 10 Jy beam^{-1}, whereas 30 masers have intensities lower than 250 mJy beam^{-1}. Note, however, that of the 15 masers observed at 25.018 GHz toward Orion-KL that are listed in Table 3.2, 12 were also observed at 24.959 GHz, as well as another one that was not observed at 25.018 GHz (Johnston et al. 1992). Seven of these were in the 1-10 Jy beam^{-1} range, and six had intensities higher than 10 Jy beam^{-1}, the highest being 84.5 Jy beam^{-1}. The masers reported in this thesis toward W51A appear to be on the lower end of this spread in intensities, with 213 mJy beam^{-1} for the 24.959 GHz maser and 365 mJy beam^{-1} for the 25.018 GHz maser (see Table 3.1).

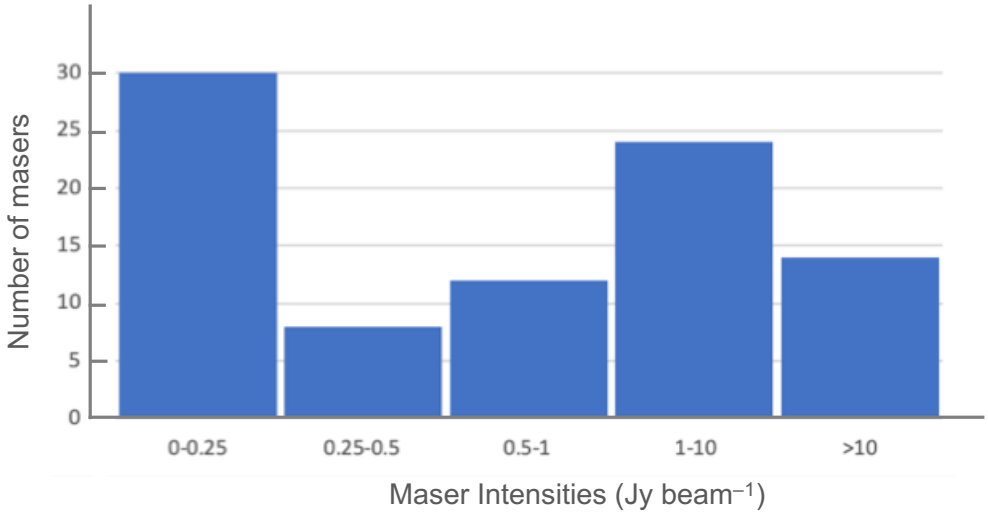

Figure 4.3: Histogram of maser intensities based on data from `maserdb.net`.

4.3 Coincidence with other maser species

There is 44 GHz emission located very close to the 25 GHz maser position, as seen in Figure 3.6; it could be a maser, or thermal emission, or a combination of both. The 44 GHz emission peaks at $19^{\rm h}\ 23^{\rm m}\ 43\overset{\rm s}{.}78$, $14^\circ\ 30'\ 15\overset{''}{.}68$, only $0.13''$ away from the location of the 25 GHz masers, which is within the beam width. However, the $v_{\rm LSR}$ of the 44 GHz emission peak, and its velocity extent, are significantly different from the $v_{\rm LSR}$ and velocity extent of the 25 GHz masers (e.g., Figure 3.6). We interpret this to mean that the 44 GHz emission arises in a different clump of gas from the 25 GHz emission. Effectively, therefore, there is no 44 GHz emission, maser or thermal, that coincides with the 25 GHz maser position.

As shown in Figure 3.4 there is no 36 GHz emission located at the 25 GHz maser position either. Again, there may be thermal or weak maser emission present toward the same position, but the $v_{\rm LSR}$ and linewidth of the 36 GHz peak differs from the $v_{\rm LSR}$ and linewidth of the 25 GHz maser. It is possible that the 36 GHz emission

is coming from the same clump as the 44 GHz emission since they share a similar velocity offset from the $v_{\rm LSR}$ of the 25 GHz masers. The 36 GHz emission is weaker than the 44 GHz almost by a factor of 10. Again, however, there is no 36 GHz maser or thermal source coincident with the 25 GHz maser position.

No Class II CH_3OH maser is coincident with the position of 25 GHz maser emission. This is not surprising since Class I CH_3OH masers are generally offset from Class II CH_3OH masers. The nearest 6.67 GHz Class II CH_3OH maser is near $19^{\rm h}\ 23^{\rm m}\ 43\overset{\rm s}{.}84$, $14^\circ\ 30'\ 24\overset{''}{.}79$ (Etoka et al. 2012), an angular separation of $9.21''$ from the position of the 25 GHz maser observed for this thesis. At the adopted distance of 5.4 kpc to W51A (Sato et al. 2010), this is equivalent to a projected distance of 0.24 pc.

A search on `maserdb.net` did not turn up any other maser species at the position of the 25 GHz masers observed for this thesis. The search was then expanded. A H_2O maser was found to be located about $5.3''$ to the north (Forster & Caswell 1999), a projected distance of 0.14 pc from the location of the 25 GHz masers. A 1720 MHz OH maser is located about $11.5''$ to the north and east of the 25 GHz maser position (Ruiz-Velasco et al. 2016), a projected distance of about 0.3 pc. Both these types of masers are known to be collisionally excited.

4.4 Characteristics of the maser region

Observations of the high mass star forming region W51A at 25 GHz have revealed Class I CH_3OH masers at 24.959 and 25.018 GHz that are concurrent in position and velocity, implying that they originate in the same clump of gas. At the same position, both 44 GHz emission and weak 36 GHz emission are also present, although not in the same velocity range as the 25 GHz maser emission. This can be interpreted to imply that the 44 GHz and 36 GHz emission likely originates from a different

clump of gas than the one responsible for the 25 GHz masers. Other than this, the location appears to be a curiously uncrowded region in what is otherwise a very cluttered region of star formation activity. The nearest water maser is 5.3″ to the north and there is a 1720 MHz OH maser located about 11.5″ to the north and east (Section 4.3). Nevertheless, the presence of collisionally excited masers like H_2O and 1720 MHz OH is well within the expected limits, since at the 5.4 kpc distance to W51, the OH maser is only 0.3 pc from the 25 GHz maser location; Class I CH_3OH masers in star forming regions are generally offset by 0.1-1 pc from radio continuum and infrared sources (Kurtz et al. 2004; Voronkov et al. 2014).

Two different scenarios exist regarding the location of the 25 GHz CH_3OH masers. One possibility is that the location of the 6.67 GHz Class II CH_3OH maser 0.24 pc away is the location of the protostar causing the outflow in which the 25 GHz masers are excited. The fact that two radio continuum sources are located very close to the Class II CH_3OH maser lends credence to this scenario. Using the position from Ginsburg et al. (2016), source e1 shown in Figure 1.4 is 0.87″ to the west and 1.31″ to the north of the 6.67 GHz Class II maser, only 0.04 pc away. Source e3 (Figure 1.4) is 0.09″ to the south of the 6.67 GHz Class II maser, a distance of only 0.002 pc. Since e1 and e3 are ionized hydrogen regions (Ginsburg et al. 2016), this would imply that 25 GHz CH_3OH masers are present at significantly late stages of the high mass star formation process, and are concurrent with Class II CH_3OH masers and H_2O masers.

Another possibility is that 25 GHz CH_3OH masers occur very early in the star formation process, long before H_2O and Class II CH_3OH masers are excited, and that a hitherto undiscovered protostar is causing the outflow in which these 25 GHz masers are excited. Mass estimates reveal that the W51A region has a significant proportion of high mass stars in the process of formation that have not yet revealed themselves.

Images in the J-band (1.235 μm) and H-band (1.662 μm) of the Two-Micron All-Sky Survey (2MASS) did not reveal any sources at or close to the location of the 25 GHz maser position, but at K_s-band (2.159 μm), there is a hint of a very faint source; this is shown in Figure 4.4. In the deeper UKIDSS (UKIRT Infrared Deep Sky Survey; UKIRT is the United Kingdom Infrared Telescope) K-band (2.2 μm) image, the faint source shows up with better visibility.

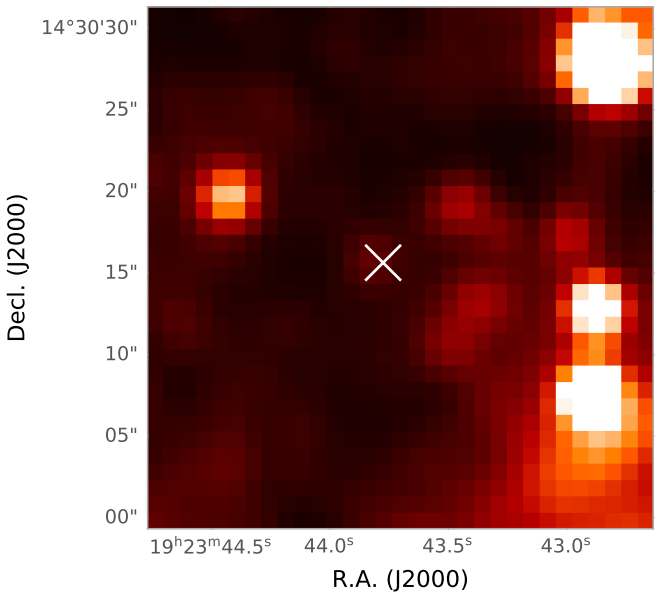

Figure 4.4: Figure showing the environment of the 25 GHz maser position in the K_s-band of the Two-Micron All-Sky Survey (2MASS). The white cross marks the 25 GHz Class I CH_3OH maser position.

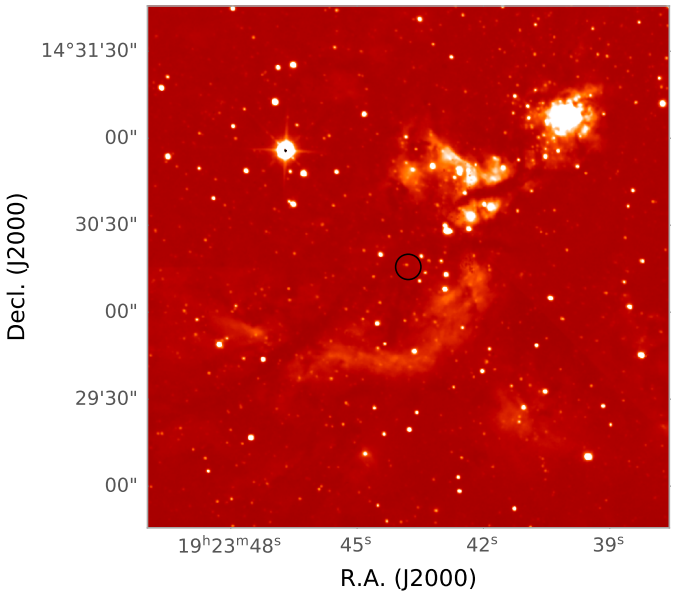

Figure 4.5: Figure showing the environment of the 25 GHz maser position in the K-band of the UKIDSS, the next-generation near-infrared sky survey that is deeper than the 2MASS survey. The center of the black circle marks the position of the 25 GHz Class I CH_3OH masers.

Finally, we explore what the presence of these 25 GHz masers tells us about the molecular gas in the region. We use the expression from Johnston et al. (1992) that the column density N_L in the lower level of the 25 GHz CH_3OH maser transition is given by

$$\frac{N_L}{T_{\rm ex}} = 1.586 \times 10^{13} \left(\tau \, \Delta v\right) \tag{4.8}$$

where τ is the optical depth of the maser line, Δv is the FWHM velocity linewidth, and $T_{\rm ex}$ is the excitation temperature of the maser transition. Modeling by Nesterenok (2021) gives an optical depth of $\tau = 0.8$ for the 25.018 GHz line. The FWHM velocity width for the 25.018 GHz maser is $\Delta v = 0.34$ km s^{-1} (Table 3.1). The excitation temperature of the maser transition is unknown, but Johnston et al. (1992) state that a reasonable value for $T_{\rm ex}$ is between 1 K and 10 K. Calculating N_L with these values gives $N_L = 4.3 \times 10^{12}$ cm^{-2} for $T_{\rm ex} = 1$ K or 4.3×10^{13} cm^{-2} for $T_{\rm ex} = 10$ K. Johnston et al. (1992) also find that the lower level of the 25.018 GHz maser contains 0.6% of the methanol population. We can use this to find the column density of methanol, $N_{\rm CH_3OH}$, by multiplying N_L by (100/0.6) to get $N_{\rm CH_3OH} = 7 \times 10^{14}$ cm^{-2} to 7×10^{15} cm^{-2} for $T_{\rm ex} = 1$ - 10 K respectively. Next, $N_{\rm CH_3OH}$ can be converted to $n_{\rm CH_3OH}$, the (particle) density for methanol in the maser region, by dividing $N_{\rm CH_3OH}$ by L, the size of the maser region. From the AIPS task JMFIT (Section 4.1), the 25.018 GHz maser size was found to be $0.44'' \times 0.31''$. At a distance of 5.4 kpc to W51, this gives a size $\sim 10^{16}$ cm. Dividing $N_{\rm CH_3OH}$ by this size then gives the density of methanol in the 25 GHz maser region to be $n_{\rm CH_3OH} = 0.07$ cm^{-3} (for $T_{\rm ex} = 1$ K) to 0.7 cm^{-3} (for $T_{\rm ex} = 10$ K). Menten et al. (1988) determined the ratio of $n_{\rm CH_3OH}$ to the molecular hydrogen density ($n_{\rm H_2}$) to be in the range 10^{-6} to 10^{-9} for thermally excited methanol. Using the middle value of 5×10^{-7} in this range, we find that the molecular hydrogen density in the maser region is $n_{\rm H_2} = 10^5$ cm^{-3} for $T_{\rm ex} = 1$ K and $n_{\rm H_2} = 10^6$ cm^{-3} for $T_{\rm ex} = 10$ K. At the shock interfaces where these masers form, the gas is compressed by at least a factor

of 10, which means that the molecular hydrogen density in the pre-shock regions is 10^4 cm^{-3} for $T_{\rm ex} = 1$ K and 10^5 cm^{-3} for $T_{\rm ex} = 10$ K.

Nesterenok (2021) found from numerical modeling that whereas 44 GHz and 36 GHz masers can be pumped in regions of pre-shock gas density of 10^4 cm^{-3}, 25 GHz Class I CH_3OH masers are optimally pumped in regions of higher pre-shock gas density $\sim 10^5$ cm^{-3}. This is consistent with the finding by Leurini et al. (2016), and later by Leurini & Menten (2018), that 25 GHz masers trace higher densities than 44 GHz and 36 GHz CH_3OH masers. Our calculated value of $n_{\rm H_2} = 10^5$ cm^{-3} in the pre-shock gas is consistent with this finding by Nesterenok (2021) if the excitation temperature is $T_{\rm ex} = 10$ K. If, instead, the excitation temperature is $T_{\rm ex} = 1$ K, a molecular hydrogen density of 10^5 cm^{-3} in the pre-shock gas would require an abundance ratio $n_{\rm CH_3OH}/n_{\rm H_2} = 7 \times 10^{-8}$, which is still within the lower range of the abundance ratio found by Menten et al. (1988).

CHAPTER 5

Conclusions and Future Work

Observations of 25 GHz Class I methanol masers toward the high mass star forming region W51A have been presented in this thesis. W51A contains some of the most active sites of high mass star formation in the Galaxy. High mass stars are an important constituent of the Universe, in large part due to their unique role in creating and seeding the galaxy with heavy elements. The formation of high mass stars is a very active area of study and remains an unsolved problem, in part because high mass stars are far away and tend to form in clusters, making observation of the various stages of their formation difficult and possible only at very high angular resolution. Masers are an effective tool to observe high mass star forming regions because masers are compact and bright objects that can be imaged with high angular resolution at large distances. The more we know about masers and their characteristics, the better we can leverage them to observe the high mass star formation process.

Observations with the VLA have revealed a Class I CH_3OH maser at 24.959 GHz toward the high mass star forming region W51A. A Class I CH_3OH maser at 25.018 GHz is coincident in position with this maser. The intensity of the 24.959 GHz maser peaks at 213 mJy beam^{-1} while the intensity of the 25.018 GHz maser peaks at 365 mJy beam^{-1}, about 1.7 times higher. The center velocity and line widths of both masers are similar and coincident within the channel spacing of the observations, with a $v_{\rm LSR}$ of 58.83 km s^{-1} and FWHM line width of 0.32 km s^{-1} for the 24.959 GHz

maser, and a $v_{\rm LSR}$ of 58.77 km s^{-1} and FWHM line width of 0.34 km s^{-1} for the 25.018 GHz maser. The narrow velocity line widths and compact sizes suggest that these two objects are masers. Calculations revealed a high brightness temperature of $T_b = 3579$ K and 5901 K for the 24.959 GHz and 25.018 GHz objects respectively, confirming that they are indeed masers. Both masers were found to be unsaturated.

Emission at 44 GHz that could be a maser, or thermal emission, or a combination of both was discovered very close to the 25 GHz maser position and almost coincident with it. However, the peak velocity and velocity extent of the 44 GHz maser emission is significantly different from that of the 25 GHz masers. Emission at 36 GHz that is coincident in position and velocity extent with the 44 GHz emission was also detected; it is likely thermal emission but may contain some weak maser emission. We interpret the 25 GHz emission as arising from a clump of velocity-coherent gas that is distinct from, but along the same line of sight as, the parcel of gas that gives rise to the 44 GHz and 36 GHz emission.

Archival data obtained from the website `maserdb.neet` provided known 25 GHz masers for comparison. Only 20 objects are associated with 25 GHz CH_3OH maser emission compared to 497 objects in which 44 GHz CH_3OH masers have been observed, attesting to the rarity of the 25 GHz maser emission process. A total of 88 masers have been observed toward these 20 objects, with a significant population having low peak intensities. Only 14 masers have intensities higher than 10 Jy beam^{-1}; the highest intensity observed is 100.8 Jy beam^{-1}. A significant number of 25 GHz masers, 38 in number, have intensities lower than 0.5 Jy beam^{-1} and the 24.959 and 25.018 GHz masers observed for this thesis toward W51A fall into this range.

The general vicinity of the 25 GHz Class I CH_3OH maser position was examined for the presence of other sources of interest. No H_2O or 1720 MHz emission that

is also collisionally excited in shocks is present at the 25 GHz maser position. The closest H_2O maser is located 0.14 pc away to the north, and the closest 1720 MHz OH maser is located 0.3 pc away to the north and east of the 25 GHz CH_3OH maser. The closest 6.67 GHz Class II CH_3OH maser is offset 0.24 pc to the north and east of the 25 GHz Class I CH_3OH maser position.

Characteristics of the maser emission and investigation of its surroundings allows us to propose two scenarios. In the first, a protostar located in the vicinity of the 6.67 Class II CH_3OH maser is driving an outflow toward the south. The 25 GHz Class I CH_3OH maser is formed by collisional excitation in this outflow. Indeed, there are two H II regions in the immediate vicinity of the 6.67 GHz Class II CH_3OH maser that could be the location of the protostar. In this scenario, the 25 GHz Class I maser is present at a significantly late stage at which the high mass protostar has formed an ionized hydrogen region around it. In the second scenario, the 25 GHz Class I CH_3OH maser is formed very early in the star formation process and is being excited in the outflow of a high mass protostar that has not yet been identified. In this scenario, the water maser and Class II maser to the north have no connection to the 25 GHz Class I maser. Support for this scenario comes from a very faint source in the 2MASS K_s band, which is more prominent in the deeper UKIDSS survey at the 2.2 μm K-band, and because several observations have pointed to an as-yet undiscovered population of early-stage high mass protostars in W51A, based on mass estimates.

Finally, we explore what the presence of the 25 GHz CH_3OH masers tells us about the molecular gas in the region. Using the observed FWHM line width of the maser, a value for the optical depth from maser modeling, and an assumed value for the excitation temperature, the column density of methanol in the maser region is estimated to be $N_{CH_3OH} = 7 \times 10^{14}$ cm^{-2} for $T_{ex} = 1$ K, and $N_{CH_3OH} = 7 \times 10^{15}$

cm^{-2} for $T_{ex} = 10$ K. Dividing N_{CH_3OH} by the observed size of the maser gives the column density of methanol in the maser region, and using the ratio of abundance of methanol to molecular hydrogen measured for thermally excited methanol yields the molecular hydrogen column density in the maser region. Assuming a factor of 10 compression in the shock, this result can then be used to estimate the pre-shock molecular hydrogen density, which was determined to be 10^5 cm^{-3} for $T = 10$ K. This is in agreement with numerical models that find that 25 GHz Class I CH_3OH masers are optimally pumped in regions of pre-shock density 10^5 cm^{-3}.

Future work to follow up on this thesis could take several directions. Some astronomers have taken the position that the claimed rarity of 25 GHz Class I CH_3OH masers is not true and is merely a result of not looking in the right places. A targeted search of high mass star forming regions might possibly yield a much larger population of 25 GHz CH_3OH masers. Another direction could be to verify whether 25 GHz masers are unsaturated. If so, they are likely to vary, and it might be possible to tie this variation to changes in the pump, which could in turn lead to insights into activity in the star forming region. Deep interferometric observations of a large sample of 25 GHz masers might also yield significantly better physical insight into their environments and help to unravel some of the mysteries of the high mass star formation process. Finally, if a sufficient population of high intensity 25 GHz masers were found, it would be possible to target them for the Zeeman effect to measure magnetic fields in these high mass star forming regions.

REFERENCES

Barrett, A. H., Schwartz, P. R., & Waters, J. W. 1971, ApJ, 168, L101

Batrla, W., Matthews, H. E., Menten, K. M., et al. 1987, Nature, 326, 49

Baudry, A., Humphreys, E. M. L., Herpin, F., et al. 2018, A&A, 609, A25

Cragg, D. M., Sobolev, A. M., & Godfrey, P. D. 2005, MNRAS, 360, 533

Eden, D. J., Moore, T. J. T., Urquhart, J. S., et al. 2018, MNRAS, 477, 3369

Eldridge, J. J. & Stanway, E. R. 2022, ARA&A, 60, 455

Elitzur, M. 1992, ARA&A, 30, 75

Etoka, S., Gray, M. D., & Fuller, G. A. 2012, MNRAS, 423, 647

Forster, J. R. & Caswell, J. L. 1999, A&AS, 137, 43

Ginsburg, A., Bally, J., Battersby, C., et al. 2015, A&A, 573, A106

Ginsburg, A., Goss, W. M., Goddi, C., et al. 2016, A&A, 595, A27

Ginsburg, A., Goddi, C., Kruijssen, J. M. D., et al. 2017, ApJ, 842, 92

Goddi, C., Ginsburg, A., & Zhang, Q. 2016, A&A, 589, A44

Goedhart, S., Gaylard, M. J., & Walt, D. J. 2005, Ap&SS, 295, 197

Johnston, K. J., Gaume, R., Stolovy, S., et al. 1992, ApJ, 385, 232

Kogan, L. & Slysh, V. 1998, ApJ, 497, 800

Kundu, M. R. & Velusamy, T. 1967, Annales d'Astrophysique, 30, 59

Kurtz, S., Hofner, P., & Álvarez, C. V. 2004, ApJS, 155, 149

Hagiwara, Y., Horiuchi, S., Doi, A., et al. 2016, ApJ, 827, 69

Ladeyschikov, D. A., Bayandina, O. S., & Sobolev, A. M. 2019, AJ, 158, 233

Leurini, S., Menten, K. M., & Walmsley, C. M. 2016, A&A, 592, A31

Leurini, S. & Menten, K. M. 2018, Astrophysical Masers: Unlocking the Mysteries of the Universe, 336, 17

Lim, W. & De Buizer, J. M. 2019, ApJ, 873, 51

MacKay, D., Thompson M., & Urquhart, J. 2023, Case Studies in Star Formation: A Molecular Astronomy Perspective. Cambridge: Cambridge University Press

Mehringer, D. M. 1994, ApJS, 91, 713

Menten, K. M., Walmsley, C. M., Henkel, C., et al. 1986, A&A, 157, 318

Menten, K. M., Walmsley, C. M., Henkel, C., et al. 1988, A&A, 198, 253

Menten, K. M. 1991, ApJ, 380, L75

Nesterenok, A. V. 2021, Journal of Physics Conference Series, 2103, 012012

Nguyen, H., Rugel, M. R., Murugeshan, C., et al. 2022, A&A, 666, A59

Reid, M. J. & Moran, J. M. 1981, ARA&A, 19, 231

Richards, A. M. S., Sobolev, A., Baudry, A., et al. 2020, Advances in Space Research, 65, 780

Ruiz-Velasco, A. E., Felli, D., Migenes, V., et al. 2016, ApJ, 822, 101

Sato, M., Reid, M. J., Brunthaler, A., et al. 2010, ApJ, 720, 1055

Sjouwerman, L. O., Pihlström, Y. M., & Fish, V. L. 2010, ApJ, 710, L111

Towner, A. P. M., Brogan, C. L., Hunter, T. R., et al. 2017, ApJS, 230, 22

Voronkov, M. A., Sobolev, A. M., Ellingsen, S. P., et al. 2005, MNRAS, 362, 995

Voronkov, M. A., Brooks, K. J., Sobolev, A. M., et al. 2006, MNRAS, 373, 411

Voronkov, M. A., Walsh, A. J., Caswell, J. L., et al. 2011, MNRAS, 413, 2339

Voronkov, M. A., Caswell, J. L., Ellingsen, S. P., et al. 2014, MNRAS, 439, 2584

Wilson, T. L., Mezger, P. G., Gardner, F. F., et al. 1970, Astrophys. Lett., 5, 99

Wynn-Williams, C. G., Becklin, E. E., & Neugebauer, G. 1974, ApJ, 187, 473

Zinnecker, H. & Yorke, H. W. 2007, ARA&A, 45, 481